(will be inserted by hand later)

Your thesaurus codes are:
06 (02.13.3; 08.16.4; 08.03.4; 08.12.1; 08.22.3; 13.19.5)

ASTRONOMY AND ASTROPHYSICS

Six years of short-spaced monitoring of the v=1 and v=2 J=1–0 ^{28}SiO maser emission in evolved stars

J. Alcolea[1], J.R. Pardo[1,2,3*], V. Bujarrabal[1], R. Bachiller[1], A. Barcia[1], F. Colomer[1], J.D. Gallego[1], J. Gómez-González[1], A. del Pino[1], P. Planesas[1], S. del Río[1***], A. Rodríguez-Franco[1,4], A. del Romero[5], M. Tafalla[1], and P. de Vicente[1]**

[1] Observatorio Astronómico Nacional (OAN), Apartado 1143, E-28800 Alcalá de Henares, Spain
[2] DEMIRM/Observatoire de Paris-Meudon, 61 Avenue de l'Observatoire, 75014 Paris, France
[3] NASA-Goddard Institute for Space Studies, 2880 Broadway, New York, N.Y. 10025, USA
[4] Departamento de Matemática Aplicada II (Biomatemática), Sección Departamental de Óptica, Escuela Universitaria de Óptica, Universidad Complutense de Madrid, Av. Arcos de Jalón s/n, E-28037 Madrid, Spain
[5] Departamento de Física, Universidad de Alcalá de Henares, Campus Universitario, E-28871 Alcalá de Henares, Spain

Received 26 January 1999 / Accepted 6 July 1999

Abstract. We present the results from a monitoring of the v=1 and v=2 J=1–0 ^{28}SiO maser emission in 21 objects, covering all types of known SiO maser emitters: 13 Mira variables, 2 long period semiregulars (SRGs), 3 variable supergiants (SGs), 2 OH/IR stars, and one young stellar object. This study has been carried out with the 13.7 meter radiotelescope of the Centro Astronómico de Yebes (Guadalajara, Spain), from July 1984 to May 1990, and represents the longest and most tightly sampled monitoring of SiO masers ever published.

Our data show that for Mira-type (i.e. regular) variables, the SiO and optical light curves agree in period, and that the maxima of the SiO emission lag the optical ones by about 0.1–0.2 periods. Since a similar lag characterizes the near infrared (NIR) emission variability from these stars, we conclude that for regular variables SiO and NIR vary in phase. This result was confirmed in three objects for which NIR variability curves are available. For SRGs and SGs, we found a less systematic behavior, but when the SiO emission is periodic, its variability curve agrees with the optical one, also showing a lag between maximum epochs similar to that of Mira-type stars. The data clearly reveal other interesting details on the SiO maser variability, such as the strong intensity differences between different maxima and changes in the velocity distribution of the emission. Finally, the SiO masers associated to the young stellar object Orion IRc2 showed a double peaked spectrum with low amplitude, aperiodic variations.

Key words: masers – stars: AGB – circumstellar matter – stars: late-type – stars: variables – radio-lines: stars

1. Introduction

Maser emission from the rotational transitions of the vibrationally excited states of ^{28}SiO (SiO hereafter) has been detected in more than 500 evolved stars and also in a few star-forming regions. The variability of the SiO masers was established in the very first works on this type of emission (see e.g. Hjalmarson & Olofsson 1979; Clark et al. 1982). Soon, this variability was studied by several projects monitoring these masers from a sample of sources. Up to date, the most complete and systematic of these monitorings are those by Lane (1982), Nyman (1985), and Martínez et al. (1988). They established some characteristics of the SiO maser variability, such as the periodic variations in Mira type stars, the systematic occurrence of the SiO maxima at phase $\sim$ 0.1–0.2 with respect to the optical maxima, and the poor reproducibility of the SiO light curves. However, more systematic work covering longer periods of time with the necessary tightness, and including more sources, is necessary to shed light on other questions about this variability; in particular, on the correlation between the SiO and near infrared (NIR) light curves, the variation pattern of the SiO maser profiles, and the eventual presence of longer secondary periods.

In July 1984, a long-term short-spaced monitoring of well known SiO maser sources was started at the 13.7 meter radiotelescope of the Centro Astronómico de Yebes

Send offprint requests to: J. Alcolea (j.alcolea@oan.es)

* *Present address:* George W. Downs Laboratory of Physics, California Institute of Technology, MS 320-47, Pasadena, CA 91125, USA

** *Present address:* Instituto de Enseñanza Secundaria "Cardenal Cisneros", C/ Cardenal Sandoval y Rojas S/N, E-28802 Alcalá de Henares, Spain

*** *Present address:* Instituto Nacional de Astrofísica, Óptica y Electrónica (INAOE), Apartado Postal 51 & 216, 72000 Puebla, Pue., México

(CAY) of the Spanish National Astronomical Observatory (OAN). Two SiO maser lines have been observed, the J=1–0 rotational transitions of the v=1 and v=2 vibrationally excited states, whose respective rest frequencies are 43 122.024 and 42 820.432 MHz. At the beginning of the project, 14 sources were observed every about three weeks, but only in the v=1 line. One year later, we started monitoring also 10 of these sources in the v=2 line. By mid 1987 two additional sources were included, all 16 sources being observed in the two transitions since then. Finally, in January 1989 five more sources were added to the list, for a total of 21 sources. The selected sources cover all types of SiO maser emitters known to date. In Table 1, we list the objects included in our monitoring and some of their characteristics, namely the type of source, the spectral type, and the period and amplitude of the optical light curve (Δm_v), taken from the 4$^{\rm th}$ edition of the *General Catalogue of Variable Stars* (Kholopov et al. 1985). The starting dates for the v=1 and v=2 observations, number of spectra presented in this paper, mean time-interval of the sampling, and other characteristics of the monitoring performed for each object are presented in Table 2.

The goals of this work have been to obtain a relatively short-spaced sampling in time ($\sim$ 3 weeks) of the two selected transitions during a period of time covering several stellar cycles for Mira-type variables (5 to 7 in most cases). We succeeded on those requirements during the entire period except for a few breaks of less than 100 days, and a break of 180 days in 1988 due to major works on the 45 GHz receiver of the CAY-13.7 m radiotelescope. Thus, we are able to present a data set rather unique both by its regular time sampling and the long period of time covered. Here we present more than 1800 spectra, to be compared with the less than 300 presented in the monitorings by Lane (1982) and Nyman (1985). Preliminary results of this project, corresponding to the first two and a half years of v=1 observations, and one and a half years of v=2 observations, were published by Martínez et al. (1988).

This paper constitutes the general presentation of our SiO data set, that is also compared with the optical and NIR variability curves of the stars when available. In Sect. 2 we describe the main characteristics of the observing system. Sect. 3 is devoted to a detailed discussion of the observational procedure adopted in order to get a relative calibration of the data as good as possible over the entire project. The general description of the data and how they are presented in this paper can be found in Sect. 4, were the major results are also outlined. Sect. 5 is devoted to brief descriptions of the results obtained for the individual sources. Finally, the conclusions are summarized in Sect. 6.

2. Observations

We present observations of SiO maser emission at 7 mm wavelength during the period July 1984 – May 1990, using the 13.7 m radiotelescope of the CAY, located at Yebes, Guadalajara, Spain. We started observing 14 objects in the v=1 transition in 1984. Ten of those were observed also in v=2 since mid 1985. In 1987 the program was extended to 16 objects, observed in both v=1 and v=2 lines. Finally, after some major works on the receiver in 1988, the program was extended up to 21 objects observed in the v=1 and v=2 masers. In principle, the observations were performed every about 3 weeks, each observational run consisting in two consecutive days of observations, the first day for the v=1 line and the second one for the v=2 line.

The main characteristics of the CAY-13.7 m radiotelescope, described by Barcia et al. (1985), remained unchanged during the observing period except for those concerning the 45 GHz receiver (and the aperture efficiency of the telescope). At the beginning of the monitoring, the receiver consisted of a Schottky diode balanced mixer and a FET amplifier at room temperature, yielding a single side band (SSB) system noise antenna temperature above the atmosphere ($T^*_{\rm a,sys}$) of about 900 K. In May 1987 the performance of the mixer was improved resulting in SSB $T^*_{\rm a,sys}$ of $\sim$ 600 K. Finally, in December 1988, the receiver was replaced with a similar one but being cooled down to 20 K with a closed-cycle Helium refrigerator, with typical SSB $T^*_{\rm a,sys}$ of $\sim$ 260 K (including the $\lambda/4$ plate, see point 3 in Sect. 3). All these changes also resulted in different polarization sensitivities of the system (see again point 3 in Sect. 3). The dependence of the antenna efficiency with elevation was tested, modeled and taken into account in the calibration procedure. We note that the telescope is enclosed in a radome, inside which the air is kept in circulation to maintain a uniform temperature. This prevents differential dilatation in the main reflector that could affect the efficiency of the telescope, as well as in the supporting structure which could introduce pointing errors.

The spectrometer used during the whole period was a filterbank of 256 channels 50 kHz wide, providing a spectral resolution of 0.35 km s^{-1} at 43 GHz, although for the data presented here we have degraded the resolution to 0.7 km s^{-1} to increase their signal to noise ratio. Most of the observations were done in frequency switching mode (by switching the IF by 6.4 MHz), which reduces the effective filterbank bandwidth to $\sim$ 44 km s^{-1}. Only for three objects in our sample, VY CMa, VX Sgr, and Orion IRc2, this velocity coverage is not large enough because of their broad maser emission, resulting in difficulties for a proper baseline subtraction. For these three objects a position switching procedure was adopted, setting the "off" position 10′ away in azimuth from the star position. Note that at 43 GHz, the half-power beam width of the telescope is $\sim$ 2′.

For the calibration of the data we have followed the procedure explained in Barcia et al. (1985), that essentially uses as references an absorber at ambient temperature as hot load, and the blank sky as cold load. This

Table 1. Observed objects: characteristics

	name	spectral type	Period (days)	Δm_v	comments
Supergiants					
	VY CMa	M5		3.1	
	μ Cep	M2	730 ?	1.7	
	VX Sgr	M4–M10	732	7.5	
Semiregulars					
	GY Aql	M6–M8	204 ?[(1)]	6	
	RT Vir	M8	155 ?	1.3	
Mira Variables					
	R Aqr	M5–M9	387	6.6	Symbiotic
	R Aql	M5–M9	284	6.5	
	TX Cam	M8–M10	557	6.1	
	R Cnc	M6–M9	361	5.7	
	R Cas	M6–M10	430	8.8	
	o Cet	M5–M9	332	6.8	Mira
	χ Cyg	S6–S10	408	10.9	S-type
	U Her	M7–M10	406	6.9	
	W Hya	M7–M9	361	3.9	SRa ?
	X Hya	M7–M9	301	6.4	
	R Leo	M6–M10	310	6.9	
	R LMi	M7–M10	372	6.9	
	IK Tau	M6–M10	470	5.7	NML Tau
OH/IR Stars					
	IRC +10011	M8	660		WX Psc
	OH 26.5+0.6				
Young objects					
	Orion IRc2				

Notes: [(1)] New optical data suggest a period of $\sim$ 400 days

method directly yields data calibrated in units of antenna temperature. This is the most usual output unit in radioastronomy, but it is not appropriate when dealing with point-like non-thermal emissions, as it is the case here, for which flux units are preferred. The conversion factor from the antenna temperature scale to flux units (Jy) has been determined from observations of the planets as standard calibrators.

3. Relative data calibration

Great care on the calibration has to be taken in a project like this one, to be able to compare measurements made at very distant epochs. We adopted several observational constraints during the entire period in order to improve the relative calibration of all the measurements as much as possible. These special procedures are presented in this section.

1. Uncertainties in the detected signal due to pointing errors were specially treated for each individual observation in order to reduce them as much as possible. We made a small map of the beam response by pointing the telescope at the star's coordinates and at four other points located $\pm 30''$ off in azimuth or elevation. Assuming the beam to be Gaussian, we calculated the pointing errors from the intensities measured at the five different points (using the values of the peak or integrated area intensities as input), and corrected the flux for each observation. This procedure is useless when the signal-to-noise ratio of the individual points is low. In such cases we took as final spectrum the average of those obtained at the different positions, after correcting the intensities assuming that there were no pointing errors. Note that this five-point map procedure is less efficient than a standard observation, and therefore somewhat longer integration times are needed to attain a certain signal-to-noise ratio.
2. In order to minimize the effect of possible changes in the efficiency of the telescope with the elevation, not properly modeled, each source has been always observed at similar elevations (see Table 2). For each source, the r.m.s. of the average elevation of the individual observations is $\sim 3°$ (also see additional reasons for this observational constraint in point 3 of this section).
3. It was also taken into account the possible influence of changes in the observed polarization on the recorded

Table 2. Observational parameters

name	observational coordinates α (1950)	δ (1950)	velocity range (km s^{-1})	P.A.[1] (°) v=1;2	E.A.[2] (°) v=1;2	sampl.[3] (days) v=1;2	num. of spectra v=1;2	starting date yymmdd v=1;2	Fig.#
VY CMa	07 20 55.0	−25 40 12	−29:61[4]	−7;−8	23;23	28;36	70;51	840628;850709	2
μ Cep	21 41 58.5	+58 33 01	3:47	102;91	56;50	28;34	33;28	870522;870614	3
VX Sgr	18 05 03.0	−22 13 55	−37:53[5]	9;−2	26;26	27;31	73;30	840628;870523	4
GY Aql	19 47 25.0	−07 44 30	11:55	15;3	39;38	27;38	73;52	840713;850709	5
RT Vir	13 00 05.8	+05 27 14	−5:39	42;8	33;52	27;35	60;28	850528;870522	6
R Aqr	23 41 14.0	−15 33 42	−48:4	−5;−13	33;30	28;36	72;51	840627;850710	7
R Aql	19 03 57.7	+08 09 08	24:68	−34;−36	47;45	39;46	14;12	890110;890111	8
TX Cam	04 56 43.0	+56 06 48	−11:33	100;101	57;57	27;46	74;29	840613;870522	9
R Cnc	08 13 48.6	+11 52 52	−5:39	11;10	60;60	36;50	14;12	890110;890111	10
R Cas	23 55 52.0	+51 06 37	4:48	90;56	61;30	26;38	74;29	840613;870522	11
o Cet	02 16 49.0	−03 12 13	23:67	29;9	37;44	24;37	77;50	840626;850709	12
χ Cyg	19 48 38.4	+32 47 10	−14:30	64;64	58;58	36;53	14;12	890109;890110	13
U Her	16 23 35.0	+19 00 18	−36:8	−40;−19	57;64	27;33	72;51	840726;850709	14
W Hya	13 46 12.0	−28 07 06	17:61	−7;7	20;21	27;34	72;50	840726;850709	15
X Hya	09 33 06.7	−14 28 05	5:49	19;16	31;32	50;48	14;11	890110;890204	16
R Leo	09 44 52.2	+11 39 40	−23:21	1;−11	60;58	28;36	72;50	840726;850709	17
R LMi	09 42 35.0	+34 44 34	−22:22	65;60	64;67	27;38	73;48	840726;850709	18
IK Tau	03 50 43.6	+11 15 32	13:57	−35;−47	49;35	25;35	68;50	850124;850709	19
IRC +10011	01 03 48.0	+12 19 51	−14:30	50;45	26;32	30;48	32;25	870522;870703	20
OH 26.5+0.6	18 34 52.5	−05 26 37	5:49	17;17	41;40	46;56	12;10	890119;890110	21
Orion IRc2	05 32 47.0	−05 24 23	−39:51	6;−7	42;42	24;37	77;58	840628;840810	22

Notes: [1] Mean parallactic angle of the observations
[2] Mean elevation angle of the observations
[3] Mean sampling interval without taking into account the 180 days break in 1988
[4] V_{lsr} range from +6 to +38 km s^{-1} before December 1987
[5] V_{lsr} range from −14 to +30 km s^{-1} before December 1987

intensity variations. It has been shown that circumstellar SiO masers can present a relatively high degree of polarization. For example Clark et al. (1985) have studied the degree of linear polarization of the v=1 J=2–1 SiO transition in several strong SiO maser emitters like o Cet, W Hya, and R Leo (these three sources are included in our monitoring). They concluded that in this transition the different maser emission peaks have a well defined angle of polarization. The degree of linear polarization could reach up to 80%, with typical values of 10–30%. McIntosh et al. (1994) published measurements of the circular and linear polarization of the J=2–1 and J=1–0 v=1 SiO maser lines in the red supergiant VY CMa. Their results show up to 10% of linear polarization at some velocities, the circular polarization being always less than 5%. Barvainis et al. (1987) also found evidence of circular polarization in five circumstellar SiO masers, but at a degree smaller than 10% in all cases. We have also made polarization measurements of 43 GHz SiO masers with the CAY-13.7 m telescope (Martínez et al. 1988). Since only one receiver polarization, horizontal linear, was available, we had to measure the linear polarization of SiO masers by observing the objects at very different parallactic angles, with the drawback that the observations are not simultaneous neither performed at the same elevation. Due to these limitations, this method is unable to reliably detect linear polarization degrees smaller than 20%. However, it is useful to check the presence of highly linearly polarized SiO maser emission, which could influence our monitoring data. In almost all cases, the linear polarization degree was found to be less than 30%, mainly for the peak flux and the velocity integrated intensity (the two parameters considered for our SiO light curves, see Sect. 4).

According to the previous discussion, we decided to observe each individual star always at the same range of sidereal time, in order to maintain the same averaged parallactic angle (and also the same elevation angle, see point 2 in this section). This method ensures that the projection of the receiver linear polarization on the object is always the same.

Regarding to the polarization state, the response of the system has been as follows. Until December 1988 the receiver polarization was horizontal linear. Then, it was changed to vertical linear until May 1989, when

a $\lambda/4$ plate was placed in front of the receiver, setting the effective polarization sensitivity of the system to left-hand circular for the rest of the monitoring.
The observational method followed and the small degree of both linear and circular polarization of SiO masers ensures that we can compare the spectra corresponding to each individual object, at least for the periods mentioned above, and that the variability curves obtained correspond to changes in the intensity or polarization state of the sources.

4. The calibration for the different atmospheric conditions of each observational run is probably the most important source of uncertainty when comparisons of different individual observations have to be done. In order to reduce this uncertainty as much as possible the observations were always performed under clear sky conditions, or partially cloudy with only high stratiform clouds (that do not affect the transmission of electromagnetic waves at 7 mm). At 43 GHz, the atmospheric effects are usually dominated by O_2 absorption and, at a lower degree, by H_2O absorption ($\tau_{H_2O} \simeq \tau_{O_2}/6$ for 6 mm of integrated water vapor above the telescope; Pardo 1996). At the location of the Yebes Observatory, the atmospheric transmission at 43 GHz under good weather conditions is in any case high, $\sim$ 93% at the zenith (Cernicharo 1988; Pardo 1996). To first approximation, variations in the ambient and atmosphere temperatures are accounted for by the calibration method. From our experience at Yebes, observing molecular lines of constant intensity (thermally excited lines in molecular clouds) under different weather conditions, we conclude that the relative calibration errors in the monitoring due to atmospheric effects are smaller than 10%. This factor can be taken as an uncertainty upper limit for our data set.
5. In addition to all the cautions explained above, a thermal continuum source, the H II region W 51, has been observed twice (one at each frequency) every observing run. This was done to detect long-term changes in the whole calibration procedure during the entire observational program. The measured intensity of W 51 over the entire program shows an r.m.s. $\sim$ 10%, in agreement with the estimates previously given. No systematic neither seasonal changes were found, and therefore no corrections have been applied to the data based on the results from the observations of W 51.

4. General results

Due to the large size of the data set collected in this work, it is nearly impossible to show all the spectra in a traditional form. Instead, we will present our monitoring in a condensed way showing most of the relevant features that can be found in it. As examples, some individual spectra are displayed Fig. 1. The plots of all the data for the 21

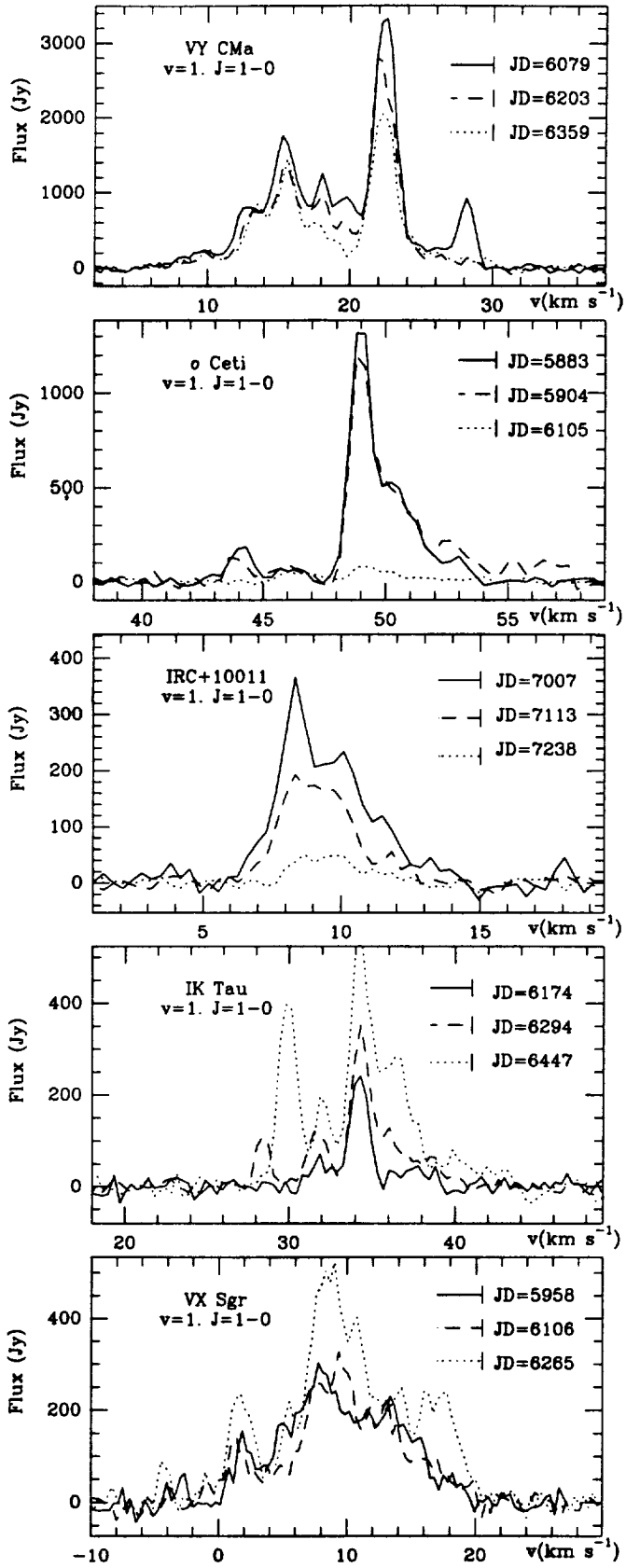

Fig. 1. Examples of individual observations of the v=1 J=1–0 maser line obtained during the monitoring for five objects: VY CMa, o Cet, IRC +10011, IK Tau, and VX Sgr

objects of the monitoring can be found in Figs. 2 to 22; they are discussed in detail object by object in Sect. 5. In these plots we show our SiO data and other simultaneous observations at different wavelengths that are of interest for our discussion. These complementary data are optical curves for most of the objects in our sample, from the AAVSO International Data Base (Mattei, priv. communication), and infrared light curves (in L' [3.79 μm] and M [4.64 μm] filters), from Le Bertre (1993) for four objects: VY CMa, R Aqr, IK Tau, and IRC+10011. The SiO data are presented in two different forms. On the right side of each figure, we show contour plots of the SiO emission (flux density in Jy) as a function of both time (Julian date, JD) and velocity (LSR) for the two lines (v=1 on the bottom and v=2 on the top). These plots allow to follow the evolution of the individual SiO maser peaks and the changes of the line shape during the observing period. In these plots we also show the variation of the velocity centroid of the total emission (thick line). Between the v=1 and v=2 contour plots, two rows of small ticks mark the dates in which the observations were performed. Note that the contours in these figures are not linearly spaced and that the noise level, usually given by the first contour, is in most cases very small compared to the peak intensity. On the left side of each figure, in addition, we have made plots of the peak flux (Jy) and (velocity) integrated flux (Jy·km s^{-1}) of the two studied SiO masers vs. time (Julian date, JD). These are the SiO light curves, to be compared with the optical and/or NIR light curves when available (displayed on the top-left corner). If possible, to ease this comparison, the epochs of optical maximum emission are shown in both SiO spectra and light curve plots by vertical lines. For the cases of IK Tau and IRC+10011, since no optical curve is shown, we have indicated the IR maxima. For OH 26.5+0.6 and Orion IRc2 no optical neither NIR maximum epochs are indicated.

The data corresponding to regular variables confirm that, in general, there is a correlation between the light curve of the observed SiO transitions and the optical variability, with a phase lag $\phi \sim 0.1$–0.2 of the first respect to the second (see, for example, Figs. 11, 12, and 18); see Martínez et al. (1988) and Hjalmarson & Olofsson (1979), for previous reports on this result. It is known that there is a similar phase lag between optical and infrared lightcurves for the type of regular variables considered here (e.g. Lockwood & Wing 1971), so the SiO maser emission and IR flux vary in phase for these objects. This is clearly confirmed for R Aqr and IK Tau, for which NIR monitorings simultaneous to our observations are presented in Figs. 7 and 19. In the infrared source IRC+10011, that is very weak in the visible, the NIR flux has a regular variability (showing a period of $\sim$ 700 days) and the SiO maser emission also vary in phase with it (see Fig. 20). The red supergiant VX Sgr and the semiregular GY Aql could show the same type of behavior (Figs. 4 and 5). See next section for more details.

Even when a periodic behavior has been found in the observed SiO maser emission, the repetitiveness from one cycle to the next is poor, for instance the maximum and minimum intensities may significantly vary from one cycle to another. Sometimes, some expected SiO maxima do not appear or are very weak (see Figs. 14 and 17).

The line profile of the SiO masers has normally several components 1–2 km s^{-1} wide over a range of $\sim$ 10 km s^{-1} (giants) to $\sim$ 20–40 km s^{-1} (supergiants). The line shape is generally similar in the two (v=1 and v=2) maser transitions. Also, we have detected sudden changes in the line shape of both lines in certain epochs (see e.g. Figs. 7, 12, and 14). No periodic change of the profile structure or velocity centroid has been found.

5. Description of the individual objects

5.1. Supergiants (SGs)

5.1.1. VY CMa (Fig. 2)

The spectral type of this star is M5 and its optical variability can reach an amplitude of 3 mag. In general this object is the strongest SiO emitter among our targets. The observations of VY CMa by Lane (1982) during 1979–1980 yielded however weaker v=1 and v=2 J=1–0 lines than in VX Sgr, W Hya, R Leo, and Orion IRc2. During our monitoring, the observed SiO maser emission of this object was always intense in the two transitions. The line profile was very stable showing several spikes, the strongest one centered at 22.5±0.5 km s^{-1} for the two transitions. The velocity of this spike agrees with the one of two vibrationally excited H_2O masers (ν_2=1 $4_{4,0}$–$5_{3,3}$ and ν_2=1 $5_{5,0}$–$6_{4,3}$) observed by Menten & Melnick (1989). These two water vapor masers have high excitation energy (3065 and 3462 K respectively) similarly to our SiO masers (1750 and 3500 K respectively for the v=1 and v=2 lines). The dominant spike in the SiO spectra published by Lane (1982) showed a different velocity, $\sim$ 20–21 km s^{-1}.

In our monitoring, the SiO variations of this object show a low contrast, i.e. a low peak flux (or total integrated area) ratio between consecutive maximum and minimum epochs, estimated to be $\sim$ 1.3. The two SiO maxima found in our observations occur more or less in phase with two optical maxima. For the peak flux curve of the v=1 line, we could find a regular variability with a period of 1000–1200 days but the minimum at JD $\sim$ 2 447 700 is not clear in the corresponding integrated flux curve. For v=2, the flux curves do not clarify the situation. Despite of this, the optical data seem to show a period of $\sim$ 1300±200 days in good agreement with the tentative period for the SiO variability. On the contrary, Herman & Habing (1985) derived a period of 989 days from observations of the 1612 MHz OH maser emission, but note that this monitoring was not simultaneous with ours. The v=2/v=1 peak flux

and integrated flux ratios are low: 0.65 and 0.55 respectively. This result is similar for other SGs. The centroid of the two lines has shown a secular shift of +2 km s^{-1} during the 2000 days of the monitoring, this variation being mainly due to intensity changes in the secondary spikes. On average, the equivalent widths (the integrated area to peak flux ratios) of the v=1 and v=2 lines are respectively 5.5 and 4.8 km s^{-1}; as it is usual in SGs (Alcolea et al. 1990) these figures are significantly higher than for red giants (Miras or semiregulars).

5.1.2. μ Cep (Fig. 3)

This star is an M2 supergiant with a small optical variation amplitude (Δm_v=1.7), and a possible period of about 730 days. Our monitoring for this star covers $\sim$ 1000 days. We see a similar increase in both v=1 and v=2 peak flux cuves by a factor of 5 to 6. During the last part of the monitoring (200–300 days) the intensity has been almost constant. If this is the beginning of a decrease in the intensity and there is a regular behavior, the period of variability should be at least of 1500 days (in disagreement with the proposed optical period). The integrated flux curves show a similar behavior. In general the value of the v=2/v=1 integrated flux ratio is low, $\sim$ 0.8, except for the epoch of minimum emission (JD 2 446 959–2 447 050) where it reaches a value of 1.3.

The line profiles of the two transitions look always very similar (one spike over a wider component). The velocity of the spike has increased 3 km s^{-1} in 1000 days, although the shift of the velocity centroid has been less than that. The v=1 equivalent width was $\sim$ 3.5–4 km s^{-1} at the beginning of the monitoring. It went down to 2.5 km s^{-1} at JD 2 447 100, just in phase with the curve of the v=2/v=1 integrated flux ratio. The v=2 equivalent width shows a similar behavior but less pronounced. In general, the values of the v=1 and v=2 equivalent widths for this star are lower than the typical values for supergiants.

5.1.3. VX Sgr (Fig. 4)

This object is an M4–M10 supergiant, which presents regular variations in the visible, with a period of 733 days and amplitudes $\Delta m_v \sim 3$ mag. The observed SiO variability is in general well correlated with the optical curve. The contrast is very low ($\sim$ 1.5) compared to those of Mira stars. The v=1 emission has a secular weakening of about a factor of 2 in 2000 days. The spectra obtained by Lane (1982) for this star show that this weakening process has been occurring since 1980 (a factor of 4–5 in total is deduced for 10 years). The short duration of the monitoring for v=2 does not allow to discuss those details for this line. The mean value of the peak flux v=2/v=1 ratio is $\sim$ 0.65; $\sim$ 0.45 for the integrated flux ratio. The mean values of the equivalent widths for the v=1 and v=2 lines are 10.5 and 8.3 km s^{-1}, respectively. All these figures are typical of SGs. The line profiles are very complex and highly variable. In general they consist of 6 or 7 peaks at velocities between -5 and +20 km s^{-1}. On average, the lifetime of the individual peaks is about 6 months, much less than the SiO period ($\sim$ 2 yr).

5.2. Semiregulars (SRGs)

5.2.1. GY Aql (Fig. 5)

The spectral type of this star is M6–M10. Its variability was not well known before the 1980's because GY Aql is weak in the optical. Now, its optical period has been established between 380 and 430 days. The amplitude of the optical variability is $\sim$ 6 mag (from $\sim$ 10 to 16 m_v). GY Aql is one of the strongest SiO emitters among SRGs. Its SiO variability is regular, with a period in agreement with the newly found optical period. The contrast is relatively high for a semiregular, $\sim$ 4–5, a value typical of Miras. The v=2/v=1 integrated flux ratio is in general $\sim$ 1. The observed line profiles often show a single peak at 34$\pm$0.5 km s^{-1}, but the equivalent widths can change quite significantly (from 1 to 6 km s^{-1}), with mean values of 3 and 2 km s^{-1} respectively for the v=1 and v=2 masers.

5.2.2. RT Vir (Fig. 6)

The optical variability of this object is practically unknown; very few data are available. The SiO maser emission is weak. The light curves for the integrated and peak fluxes and are noisy, but it is possible to see sharp changes in the intensities of the masers. In particular, note the strong increase in the SiO intensity 100–200 days after the optical burst occurred on JD 2 447 650. The mean value of the v=2/v=1 integrated flux ratio is 1.5. The line profiles show important changes in their structure. The velocity range where emission has been found is large: $\sim$ 18 km s^{-1}. The v=1 and v=2 equivalent widths are, on average, 4.5 and 3.5 km s^{-1}, respectively.

5.3. Mira Variables

5.3.1. R Aqr (Fig. 7)

This object is a symbiotic system, consisting of a Mira variable and a hot dwarf companion. It is one of the rare examples among the members of this category where SiO maser emission has been detected. Probably, the molecular shell around R Aqr is very thin, since it has not been detected in CO emission (e.g. Young 1995). The interferometric observations of the v=1 J=2–1 SiO maser in this

object by Hollis et al. (1990) showed that the maser position and that of the red giant are coincident within the error-bars of the measurements. So, one can expect that the SiO masers in this object are similar to those of other Mira variables, as it is confirmed by our data.

The SiO flux curves of this star show a good correlation with its optical variability. There is a phase lag between the SiO maximum and the optical maximum of 0.1–0.2 periods, while SiO and IR vary in phase. The contrast is moderate for a Mira: $\sim$ 3–4. The intensity of the SiO masers shows a secular increase from JD 2 446 000 to JD 2 448 000. The v=2/v=1 integrated flux ratio has also been increasing during the same period from 0.8 to 2. The velocity centroid of the maser emission has shown variations (simultaneously in the two lines) up to 6–7 km s^{-1} that are not related with the optical phase. These velocity variations are associated to very important changes in the shape of the spectra (vanishing of some maser spikes and apparition of new spikes at very different velocities; see e.g. the v=1 spectra around JD 2 446 650 and 2 447 200). The most stable peak appears at $\sim$ 27.5 km s^{-1}. The v=1 and v=2 equivalent widths show average values of 4.2 km s^{-1} and 3.8 km s^{-1}, similarly to other Miras.

5.3.2. R Aql (Fig. 8)

Although the monitoring in object is very short, the data suggest that also in this Mira star the SiO variability follows the stellar cycle. The typical phase lag between the optical and SiO curves is not clear, however. The line profiles of the two transitions are in general similar, with a v=2/v=1 integrated flux ratio of less than 1.0 (equivalent widths $\sim$ 3.5 km s^{-1}).

5.3.3. TX Cam (Fig. 9)

This giant star displays a very late spectral type, M8–M10. All SiO light curves show the characteristics of other Miras with the usual phase lag with respect to the visible. The behavior of the SiO light curves is quite regular, with a contrast of $\sim$ 6. From maximum to maximum we find differences up to a factor of 3 for the peak flux and up to a factor of 2 for the velocity integrated flux. The v=2/v=1 integrated flux ratio is $\sim$ 1 independently of the phase. The lines show the most important spike at $\sim$ 9 km s^{-1}. On average, the v=1 equivalent width is 5 km s^{-1}, 4 km s^{-1} for the v=2 line.

5.3.4. R Cnc (Fig. 10)

As for the other objects last included in our work (R Aql, χ Cyg, X Hya, and OH 26.5+0.6), the monitoring presented for this M6–M9 Mira variable is probably insufficient for concluding on the nature of its SiO variability. Nevertheless, the data presented here suggest that, also in this star, the SiO maser intensity follows the optical variations, with the typical phase lag of about 0.2 stellar cycles. The profiles of the two lines are not always similar, and the equivalent widths are $\sim$ 3.5 km s^{-1}.

5.3.5. R Cas (Fig. 11)

This star has a large optical variability ($\Delta m_v \sim 6$ mag) and the same holds for the SiO maser emission. The SiO flux curves in this star are typical of a Mira variable and show a contrast of $\sim$ 7. The v=2/v=1 integratd flux ratio has values between 0.5 and 1.0. The centroid of the v=2 line is, in general, placed at about 1 km s^{-1} to the red of the centroid of the v=1 line. The two lines have a similar shape, which presents strong changes during some SiO minima (see e.g. data at JD 2 446 450). The v=1 equivalent width increased from 3 km s^{-1} (JD 2 446 000) to 7 km s^{-1} (JD 2 447 300), dropped to 3 km s^{-1}, and started to increase again. The mean values of the v=1 and v=2 equivalent widths are 4 and 4.3 km s^{-1} respectively.

5.3.6. *o* Cet (Fig. 12)

This star, also known as Mira, is the prototype of this variability class, which is named after it. Its optical variability reaches an amplitude of 6.5 mag with a period of 332 days. It belongs to a multiple system and it has been shown that the v=1 J=2–1 SiO maser emission is associated to the red giant (Hollis et al. 1990). The SiO curves of this object show a large contrast ($\sim$ 4–20), the emission being undetectable during several minima, despite of that this object is in general a very strong SiO emitter. This fact, and its relative short period, makes this object the best suited for a detailed study on the SiO variability, in particular, to measure the phase lag of the SiO curves with respect to the optical one. Fig. 12 clearly shows that this phase lag is of about 0.1–0.2 periods. The intensity of the maxima has been decreasing during the monitoring suggesting the possibility of a longer secondary period: however the verification of this point would require to extend the monitoring for several more years. The v=2/v=1 integrated flux ratio is, in general, between 0.5 and 1.5. During the monitoring, the line shapes of the two transitions have been similar except for a few short periods of time. The structure of the lines suffered important changes in several epochs, sometimes in coincidence with SiO minima (see data at JD 2 2446 050, 2 2446 750, and 2 2447 400). The mean values of the v=1 and v=2 equivalent widths are 3 and 2.5 km s^{-1} respectively.

5.3.7. χ Cyg (Fig. 13)

This is the only S spectral type object in our sample. Due to the low abundance of Oxygen respect to Carbon (in

comparison with M-type stars), the SiO masers of this type of objects are weaker than those of O-rich stars (no SiO masers have been detected in C-rich stars). The period of the optical variability of χ Cyg is similar to the 500 days of duration of our monitoring. Therefore, it is very difficult to establish whether the behavior of the SiO variability is regular or not. The previous works (Lane et al. 1982; Nyman 1985) do not help in clarifying this point. The v=2 maser is in general weaker than the v=1 one, and we report its detection only during a few epochs. The SiO masers showed strong changes in the line profiles during the monitoring of this source. The v=1 equivalent width is 3.7 km s^{-1}, while for the v=2 line it is 2.7 km s^{-1} (on average).

5.3.8. U Her (Fig. 14)

The spectral type of this star is M7–M10 and the amplitude of its optical variability reaches values of about 5 mag. The observed SiO emission shows good examples of what we denominate "missing maxima", i.e. epochs where an SiO maximum is expected but does not appear with enough contrast respect to the two adjacent minima. See, for example, the cases at JD 2 446 700 and 2 447 100. The mean contrast, due to these "missing maxima", is low, $\sim$ 2.5. The v=2/v=1 integrated flux ratio does not have any regular variability and the mean value is $\sim$ 1. The centroid of the lines has a significant shift to the red between JD 2 446 700 and 2 447 100. In general, the changes of line shape are important from cycle to cycle. On average, the equivalent widths of the v=1 and v=2 SiO masers are 4.5 and 3.5 km s^{-1}, respectively.

5.3.9. W Hya (Fig. 15)

This star is sometimes classified as a semi-regular (SRa), but the optical data we show in this work are not different from those of a typical Mira star: the variations are regular, with an amplitude of $\sim$ 4 mag. The SiO line shape is quite complex. The lines have always many spikes, the most intense ones seem to appear only after the optical maxima, with the typical phase lag of 0.1–0.2 (see for example the data around JD 2 446 900). The centroids of both lines remain within a range of 5 km s^{-1} during our monitoring; there is no systematic pattern in their variability. The v=1 and v=2 line shapes have important variations and, sometimes, the profiles at the two frequencies are quite different. Emission has been observed over a wide range of velocities (18 km s^{-1}), the mean value of both equivalent widths being however moderate, 4.3 km s^{-1}.

5.3.10. X Hya (Fig. 16)

In this object the signal to noise ratio is too low and the monitoring too short as to allow a detailed study of the properties of its SiO maser variability. Anyhow, the data suggest that the SiO curves follow the stellar cycle.

5.3.11. R Leo (Fig. 17)

This star is also a typical Mira variable, but the SiO variability is not very regular. There are some SiO maxima with a phase lag of $\sim$ 0.2 respect to the optical ones, but there is also a "missing maximum" at the beginning of the monitoring. However, a Fourier analysis of the SiO variability curves yields a period that is consistent with the optical one. The two line centroids are very similar, presenting a secular shift of -4 km s^{-1} during the 6 years of our monitoring. The line shape changes frequently and, sometimes, the differences between the v=1 and v=2 maser profiles are important. On average, the equivalent width of the v=1 line is 3.9 km s^{-1}; for the v=2 one it is 3.3 km s^{-1}.

5.3.12. R LMi (Fig. 18)

This object is an M7–M10 Mira star with an optical variability amplitude of $\sim$ 5 mag. The regularity of the SiO data is good. The maxima are well defined for both v=1 and v=2 lines and the phase lag between the SiO emission and the optical is very clear. The mean SiO contrast is $\sim$ 3. The v=2/v=1 integrated flux ratio has a mean value of $\sim$ 0.7, except for the minima where it is $\sim$ 1. The centroids of the emission of the two lines change roughly in the same way. The mean value of the equivalent width of both lines is 3.6 km s^{-1}.

5.3.13. IK Tau (Fig. 19)

This star shows regular optical variations with an amplitude of $\sim$ 4.5 mag, somewhat smaller than what is typical for Mira variables. It presents a large excess of infrared emission. The SiO data are very regular with a contrast of 3–4. The integrated fluxes of the two maser lines show very similar values over the different periods. In this case we present NIR observations of the star, from which it can be seen their excellent correlation with the SiO emission curves. The v=1 and v=2 line profiles appear very similar during the whole monitoring (two peaks, one at constant velocity and the other showing a secular shift of about 2 km s^{-1} in 1700 days). Due to the stability of the line profiles in IK Tau, we have detected SiO maser emission within a velocity range of only 10 km s^{-1}. The mean values of the v=1 and v=2 equivalent widths have been 3.3 and 3.6 km s^{-1} respectively, ranging from 2 to 5 km s^{-1} during the monitoring presented here.

5.4. OH/IR objects

5.4.1. IRC +10011 (WX Psc; Fig. 20)

This is an infrared object, very probably a Mira-type variable with a very thick circumstellar envelope that makes very difficult to detect the central star at optical wavelengths. Herman & Habing (1985) have calculated a period of 632 days from a monitoring of the 1612 MHz OH maser emission in this object. Our SiO data seem to indicate a regular variation with a period of 500–600 days, in good agreement with the OH and IR periods. It is well known than in this type of objects both IR and OH maser emission vary practically in phase (see e.g. Habing 1996 and references therein). According to these data, an OH and IR maximum is predicted around JD 2 446 850. More recent NIR data from Le Bertre (1993) would indicate maxima at about JD 2 446 950 and JD 2 447 600. From our data we conclude that the SiO maser emission follows the NIR variations also in this source. The SiO contrast is moderate (~ 4). The v=2/v=1 integrated flux ratio shows a dependence with the phase, being ~ 1 during the maxima and reaching ~ 3 during the minima. The line profiles of the two transitions are very similar, with a strong change in shape around JD 2 247 500. The mean value of the equivalent width of both lines is 3.5 km s^{-1}.

5.4.2. OH 26.5+0.6 (Fig. 21)

This object is also surrounded by a very thick dust envelope and its optical counterpart has not been detected. The 1612 MHz OH maser emission measurements by Herman & Habing (1985) indicate a period of 1566 days, predicting a maximum for JD $\sim$ 2 447 960, in good agreement with the SiO maximum at JD $\sim$ 2 447 950 found in our data. We cannot conclude at this point whether the SiO variability follows the IR curve or not, but we recall that usually the OH and IR curves are closely in phase. In general the v=2 line is in this object stronger and more complex than the v=1 line. The v=2/v=1 integrated flux ratio reaches a value of 8 during the minimum, and it is ~ 2 for the maximum at JD $\sim$ 2 447 950. The v=2 equivalent width has a mean value of 4.5 km s^{-1}, while the v=1 one is only 1.7 km s^{-1}.

5.5. Young stellar objects

5.5.1. Orion IRc2 (Fig. 22)

This SiO maser is the only one in our monitoring that is not associated to an evolved star; the SiO emission in this region of massive star formation is associated with the infrared source IRc2 of the BN-KL nebula in the Orion A molecular cloud. There are only three known SiO maser sources associated to young objects in regions of very active star formation: Orion IRc2, Sgr B2(M) and W51-IRS2; the OH, H_2O, and CH_3OH masers being more common in these type of sources.

The line profiles of the v=1 and v=2 SiO masers observed in Orion IRc2 show two peaks (centered at ~ -5 and $+16$ km s^{-1}) with almost no emission in the zone in between. This line shape has been essentially maintained since the discovery of these masers in Orion IRc2 in 1973 (Snyder & Buhl 1974). From VLBI observations (Greenhill & Moran 1986), it has been shown that these two spectral components are located in two different positions in the sky, separated by $\sim$ 0.″14 (10^{15} cm for a distance to Orion A of 450–500 pc). The velocity centroid of the overall profile is about $+5-+6$ km s^{-1}, close to that of the hot core surrounding IRc2.

The observed SiO variability does not show any regularity. The variations of the two components are independent, the blue one showing a larger amplitude. Also the variation of the v=2/v=1 flux ratio has no regularity. The two main components have several sub-peaks with lifetimes of a few months. The equivalent widths of the two components are very variable in the two transitions, with values between 3 and 7 km s^{-1}.

6. Conclusions

We present the results of the most complete monitoring of ^{28}SiO maser emission in evolved stars carried out up to date, due to the regularity and short-spacing of the sampling ($\sim$ 30 days), the wide set of sources observed, and the long period of time covered (6 years). The observed transitions are the v=1 and v=2 J=1–0 lines. The sample contains a total of 21 objects, including red supergiants, semi-regular variable stars, Mira-type variables, OH/IR objects and one young stellar object. Special care has been taken to optimize the relative calibration of the data during the whole observing period. We conclude that, for each object, the relative flux uncertainty remains within $\pm$ 10%.

The data have been compared with optical and NIR light-curves. For objects known to be regular variables in the visible and/or in the IR (i.e. Mira-type and OH/IR stars), the SiO masers also appear to vary periodically, showing a period equal to the optical one in agreement with previous works, see Hjalmarson & Olofsson (1979), and Martínez et al. (1988). We have confirmed this result by a preliminary Fourier analysis of the SiO variability curves; no secondary periods have been found. We also confirm the existence of a systematic phase lag between the optical and the SiO maximun epochs, of about 0.1–0.2 periods. Of the 59 optical or IR maxima of Mira-type stars in our monitoring (excluding the S-type star χ Cyg), in 53 cases (90%) we find a well defined maximum in at least one of the SiO lines between phase 0.0 and 0.3 (with respect to the optical maximum). This phase lag is

comparable to that found between optical and IR maxima. Therefore, the SiO masers vary systematically in phase with the IR. This result is directly confirmed, in particular, for the stars R Aqr, IK Tau, and IRC +10011, for which variability curves at 4 μm simultaneous with our SiO monitoring are available. The IR maxima of these objects show a striking coincidence with the SiO ones in all cases.

However, the reproducibility of the SiO curves is often poor. The contrast (intensity ratio between consecutive maximum and minimum epochs) is strongly variable in most objects, with an average value of about 3. In *o* Cet (Mira) this parameter shows particularly high values, ranging from 4 up to 20. U Her, W Hya, and R Leo show contrasts between 1 and 3; a contrast of 1 is the extreme case in which an SiO maximum is missed, i.e. it is not clearly detected between two consecutive minima. Only 3 or 4 missing SiO maxima can be identified in Mira-type stars, in the curves of U Her, W Hya, and R Leo. On the other hand, the SiO emission of IK Tau shows a remarkably regular variability.

In supergiants and semiregular giants the variability of the SiO masers is much less regular than for Miras. In two objects, the supergiant VX Sgr and the semiregular variable GY Aql, we find nevertheless a periodic behavior quite well correlated with the optical variability (VX Sgr and GY Aql are relatively regular variables also at other wavelengths). The SiO emission from the young object Orion IRc2 shows low-amplitude, unpredictable variations.

The shape and centroid of the line profiles are also variable. However, no clear periodicity or trend is found, even for Mira variables. We notice centroid variations larger than about 5 $\mathrm{km\,s^{-1}}$ in periods of time shorter than 200 days for the stars R Aqr, U Her, and W Hya. In *o* Cet and R Leo, the line shape completely changed in time scales of this order. However in the supergiant VY CMa and the Mira variable IK Tau, the line shape has been remarkably constant during the whole observing period.

Acknowledgements. The pure observational work in this paper amounts to more than 2 000 hours of telescope time. Technical works can be estimated as taking at least the same amount of time. Such an effort would have never been possible without the participation of all the astronomers and the whole technical staff of the Yebes Observatory. In this research, we have used, and acknowledge with thanks, data from the AAVSO International Database, based on observations submitted to the AAVSO by variable star observers worldwide. We also acknowledge T. Le Bertre for providing us with the NIR observations presented in this paper. This work has been financially supported by several projects of the Spanish DGES, the last one under code PB96-0104.

References

Alcolea J., Bujarrabal V., Gómez-González J., 1990, A & A 231, 431
Barvainis R.E., McIntosh G., Predmore C.R., 1987, Nat 329, 613
Barcia A., Bujarrabal V., Gómez-González J., Martín-Pintado J., Planesas P., 1985, A & A 142, L9
Cernicharo J., 1988, Ph. D. Thesis, Université de Paris VII
Clark F.O., Troland T.H., Johnson D.R., 1982, ApJ 261, 569
Clark F.O., Troland T.H., Miller J.S., 1985, ApJ 289, 756
Greenhill L.J., Moran J.M., 1986, Ames Research Summer School on Interstellar Processes, Contributed Papers, 22
Habing H.J., 1996, A & AR 7, 97
Herman J., Habing H.J., 1985, A & AS 59, 523
Hjalmarson Å., Olofsson H., 1979, ApJ 234, L199
Hollis J.M., Wright M.C.H., Welch W.J., et al., 1990, ApJ 361, 663
Kholopov P.N., et al., 1985, General Catalogue of Variable Stars, 4th ed. Moscow
Lane A.P., 1982, Ph. D. Thesis, University of Massachusetts
Le Bertre T., 1993, A & AS 97, 729
Lockwood G.W., Wing R.F., 1971, ApJ 169, 63
McIntosh G.C., Predmore C.R., Patel N.A., 1994, ApJ 428, L29
Martínez A., Bujarrabal V., Alcolea J., 1988, A & AS 74, 273
Menten K.M., Melnick G.J., 1989, ApJ Let 341, L91
Nyman L.A., 1985, Ph. D. Thesis, Chalmers University of Technology
Pardo J.R., 1996, Ph. D. Thesis, Université Pierre et Marie Curie [Paris VI]
Snyder L.E., Buhl D., 1974, ApJ 189, L31
Young K., 1995, ApJ 445, 872

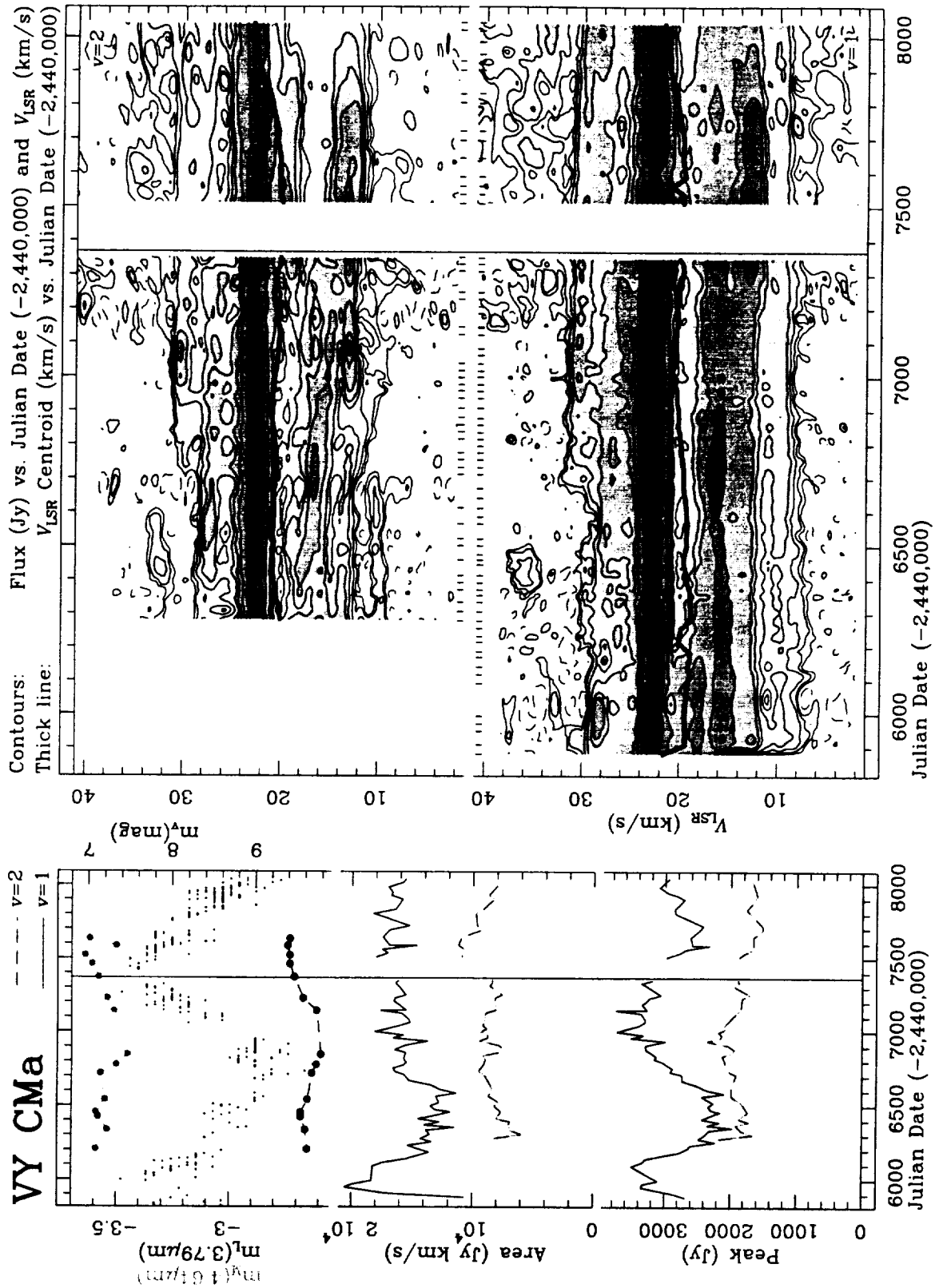

Fig. 2. Results of the SiO monitoring for the red supergiant VY CMa. On the left, optical (dots) and SiO (lines) variability curves. On the right, spectra (contours) and variability of the centroid (thick line) for the v=1 (bottom) and v=2 (top) J=1–0 maser lines. Contours for v=1 are: −25, 25, 50, 100, 200, 400, 600, 1000, 2000, and 3500 Jy. For v=2: −25, 25, 50, 100, 200, 300, 500, 1000, 1500, and 2500 Jy. In addition to the optical variability, we have also displayed an available IR monitoring of this object in L′ (big black dots) and M (big grey dots) bands

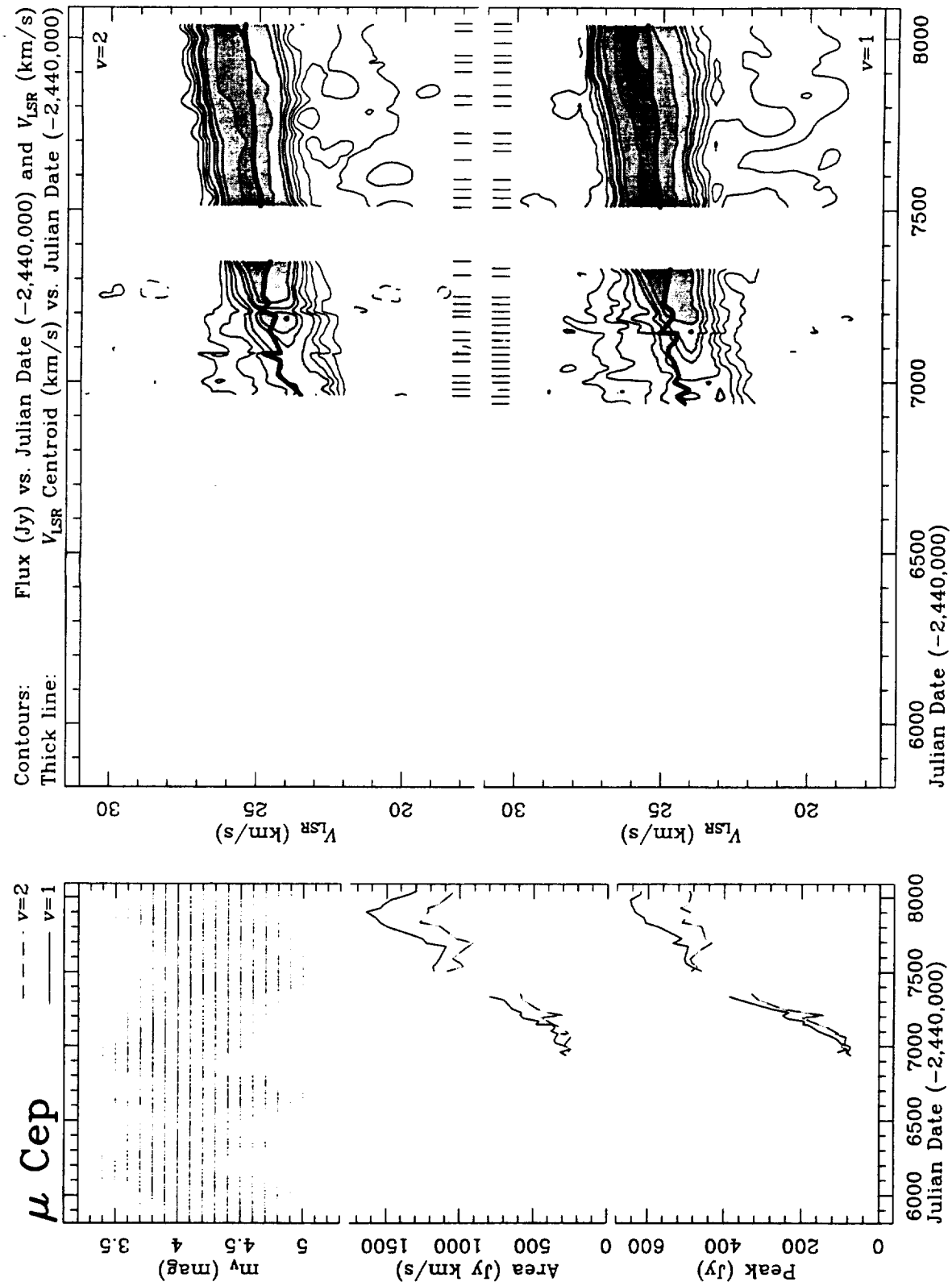

Fig. 3. Same as Fig. 2 for the red supergiant μ Cep. The contours for both v=1 and v=2 are: −15, 20, 40, 60, 80, 120, 150, 200, 400 and 600 Jy

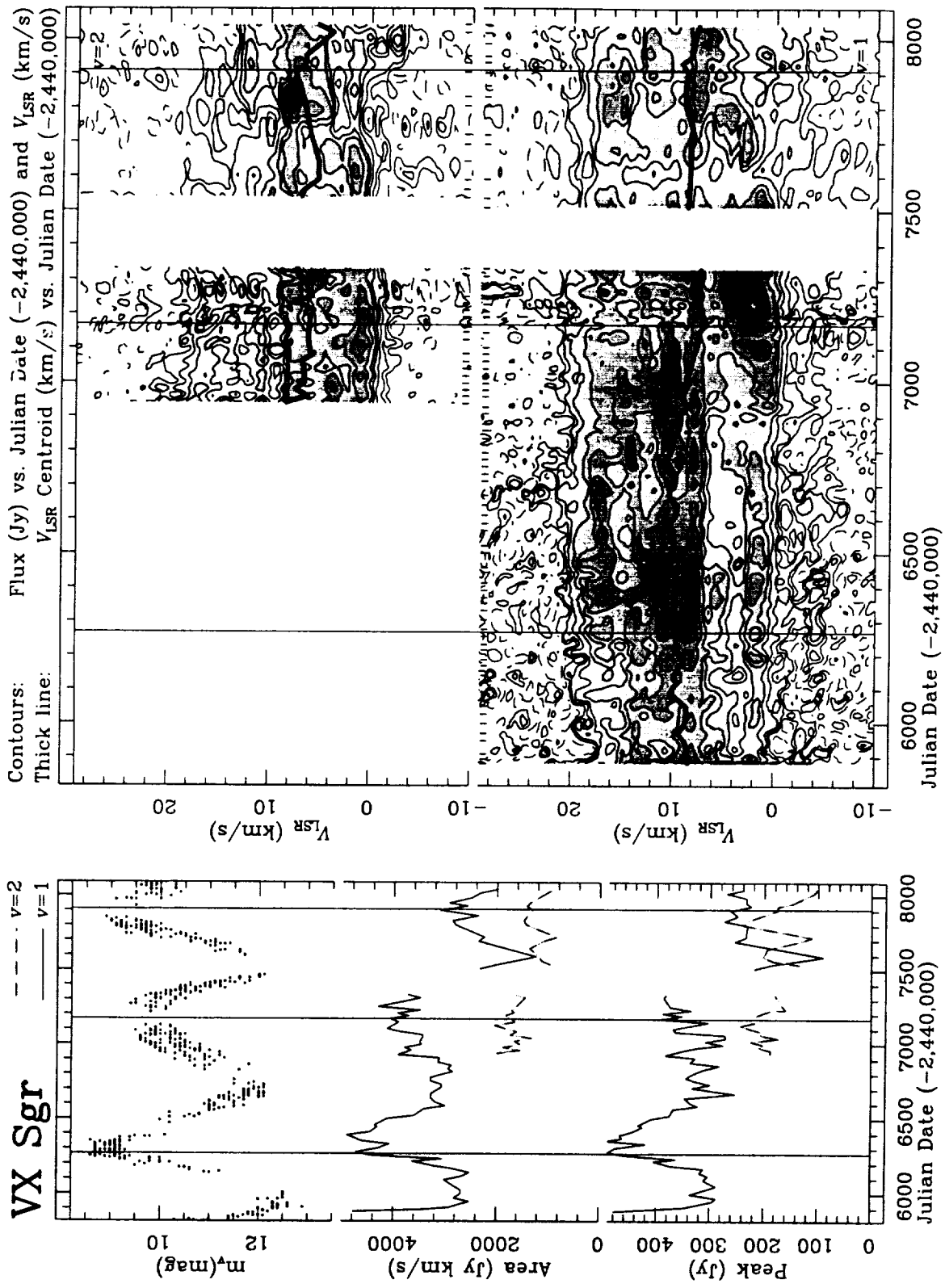

Fig. 4. Same as Fig. 2 for the supergiant regular variable VX Sgr. v=1 contours: −10, 10, 25, 50, 100, 150, 200, 300, 400, and 500 Jy. v=2 contours: −10, 10, 25, 50, 75, 100, 150, 200, 250, and 300 Jy

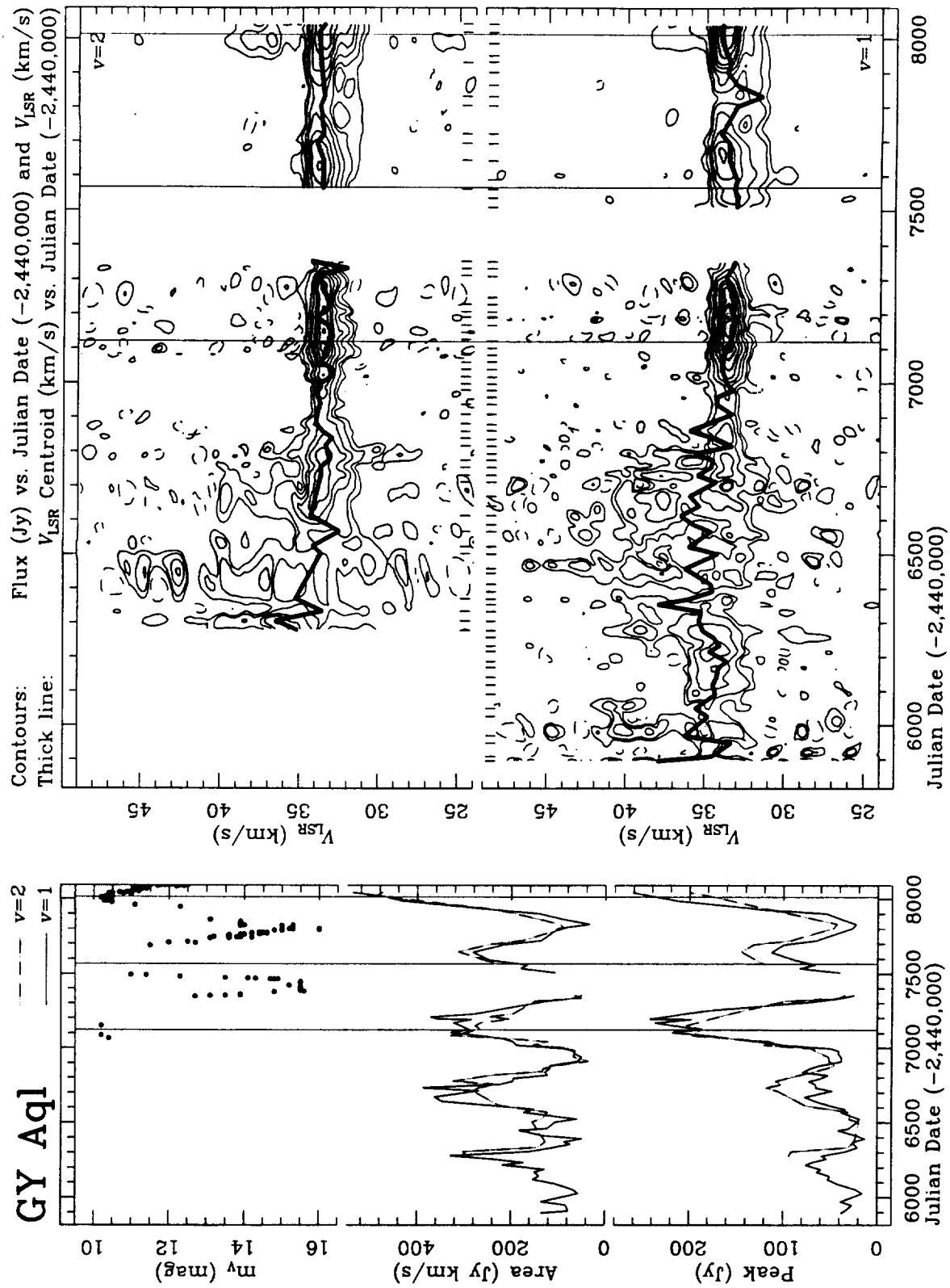

Fig. 5. Same as Fig. 2 for the semiregular variable GY Aql. v=1 contours: −10, 10, 20, 40, 60, 90, 120, 160, 200, and 250 Jy. v=2 contours: −10, 10, 20, 40, 60, 90, 120, 160, and 200 Jy

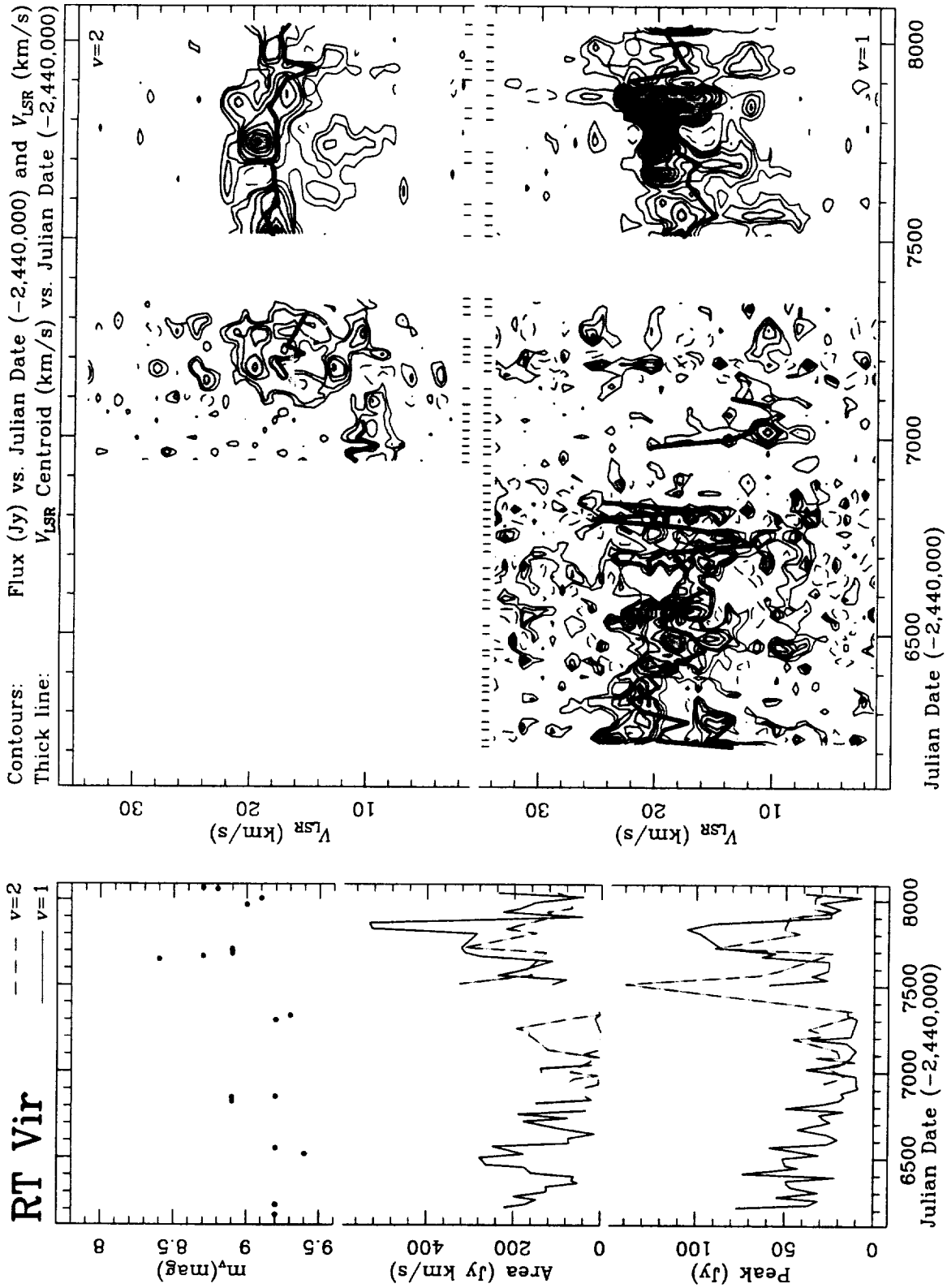

Fig. 6. Same as Fig. 2 for the semiregular variable RT Vir. v=1 contours: −10, 5, 10, 15, 20, 30, 40, 50, 75, and 100 Jy. v=2 contours: −10, 5, 10, 20, 30, 50, 75, 100, 125, and 150 Jy

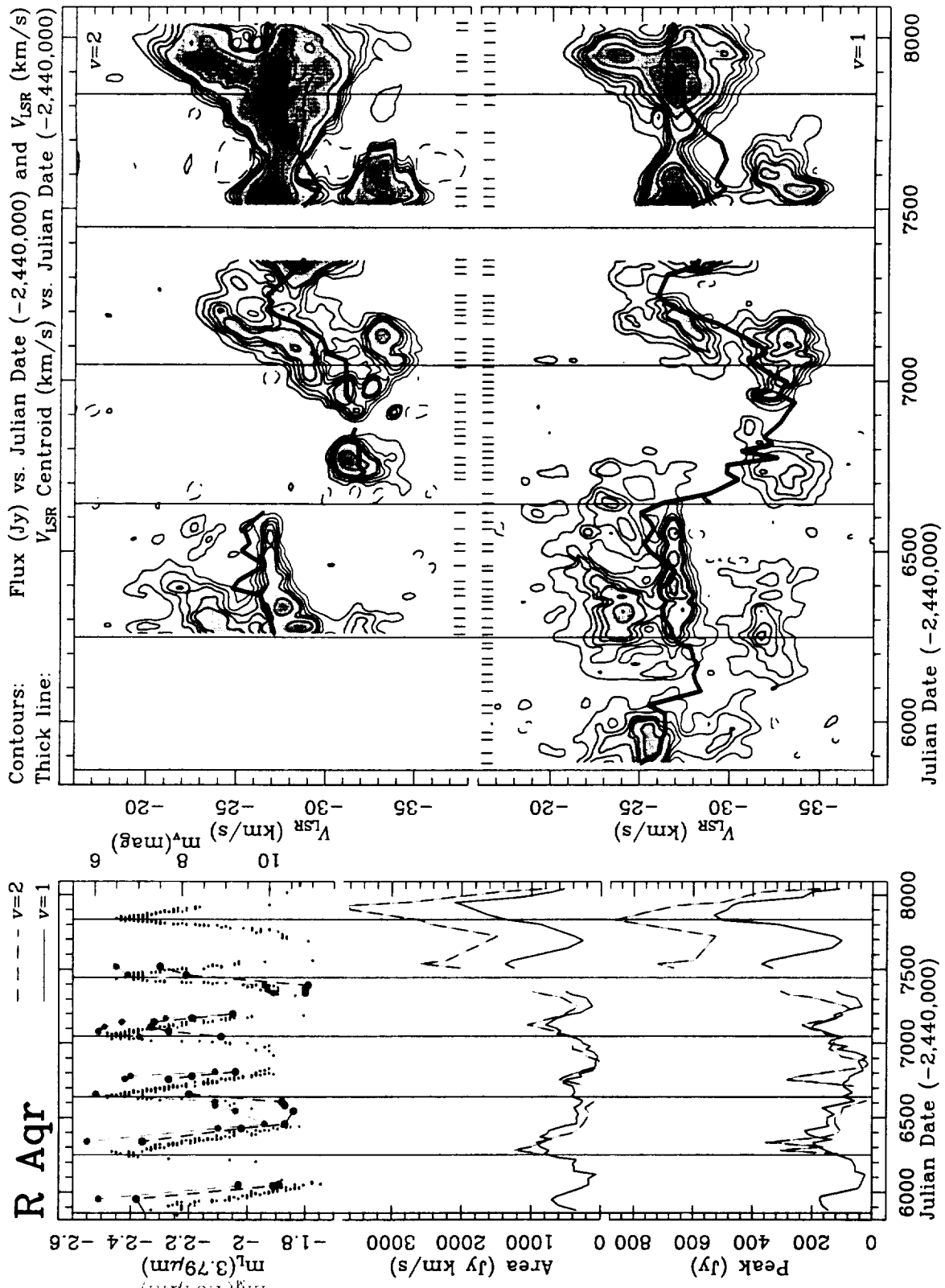

Fig. 7. Same as Fig. 2 for the Mira variable R Aqr. v=1 contours: −20, 20, 40, 60, 80, 100, 150, 200, 300, and 500 Jy. v=2 contours: −20, 20, 40, 60, 80, 100, 200, 400, 600, and 800 Jy. As for the case of VY CMa, we have also displayed IR monitorings of this object in L′ and M bands

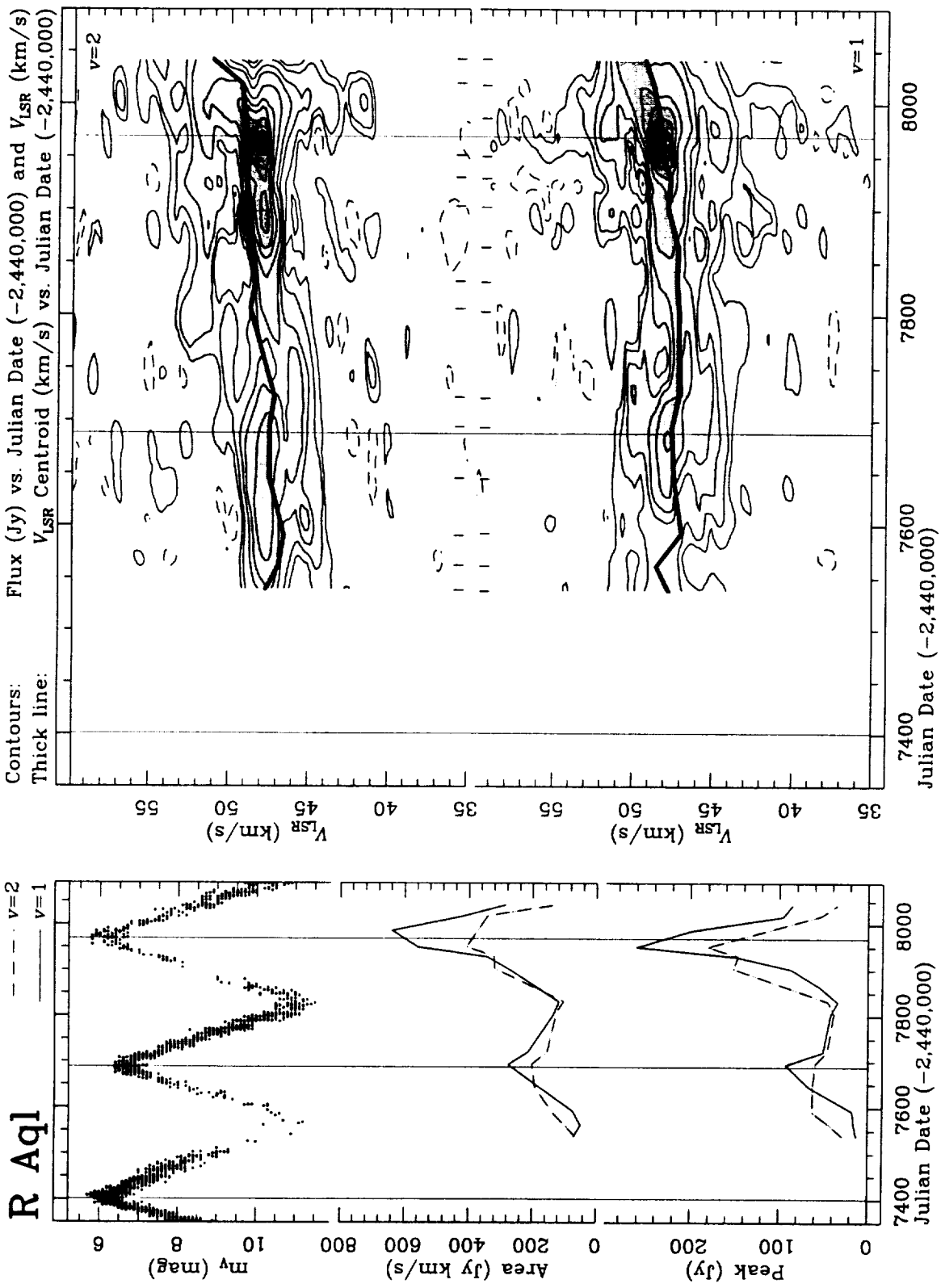

Fig. 8. Same as Fig. 2 for the Mira variable R Aql. v=1 contours: −5, 5, 10, 20, 30, 50, 100, 150, 200, and 250 Jy. v=2 contours: −5, 5, 10, 20, 30, 50, 75, 100, 140, and 180 Jy

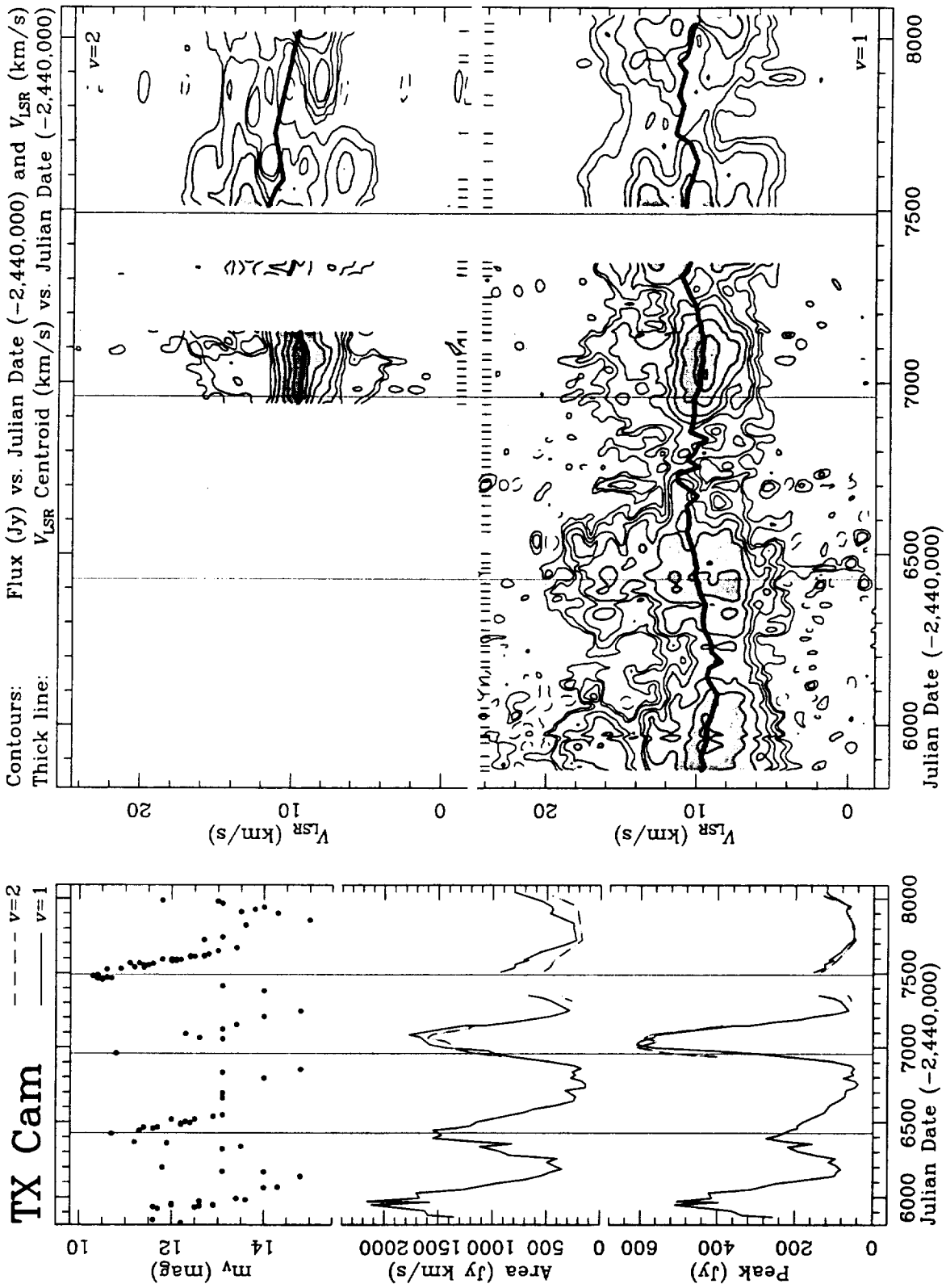

Fig. 9. Same as Fig. 2 for the Mira variable TX Cam. v=1 contours: −15, 10, 20, 40, 60, 100, 200, 400, and 600 Jy. v=2 contours: −15, 10, 20, 40, 60, 100, 200, 300, 450, and 600 Jy

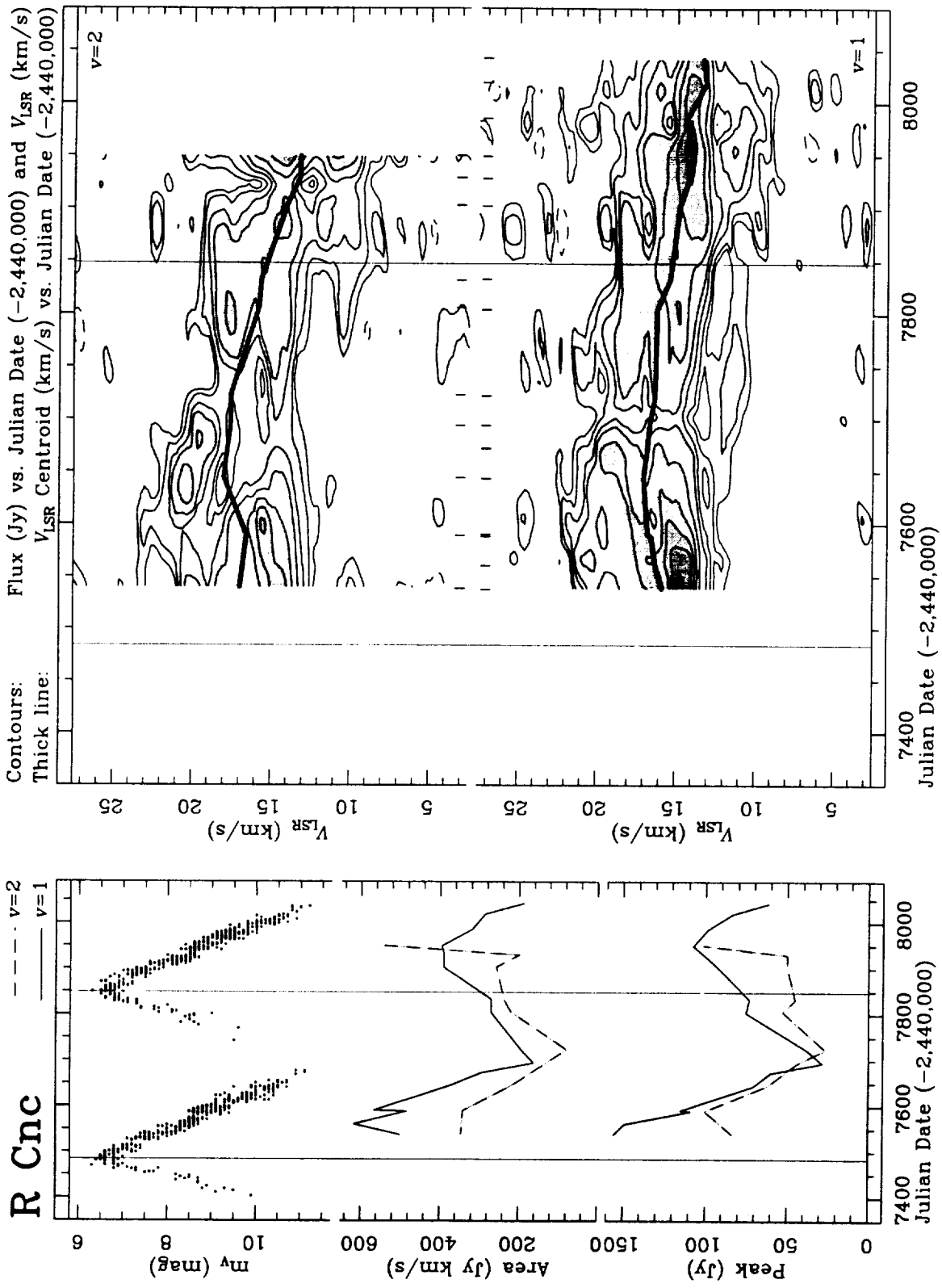

Fig. 10. Same as Fig. 2 for the Mira variable R Cnc. v=1 and v=2 contours: −10, 5, 10, 20, 30, 50, 75, 100, 125, and 150 Jy

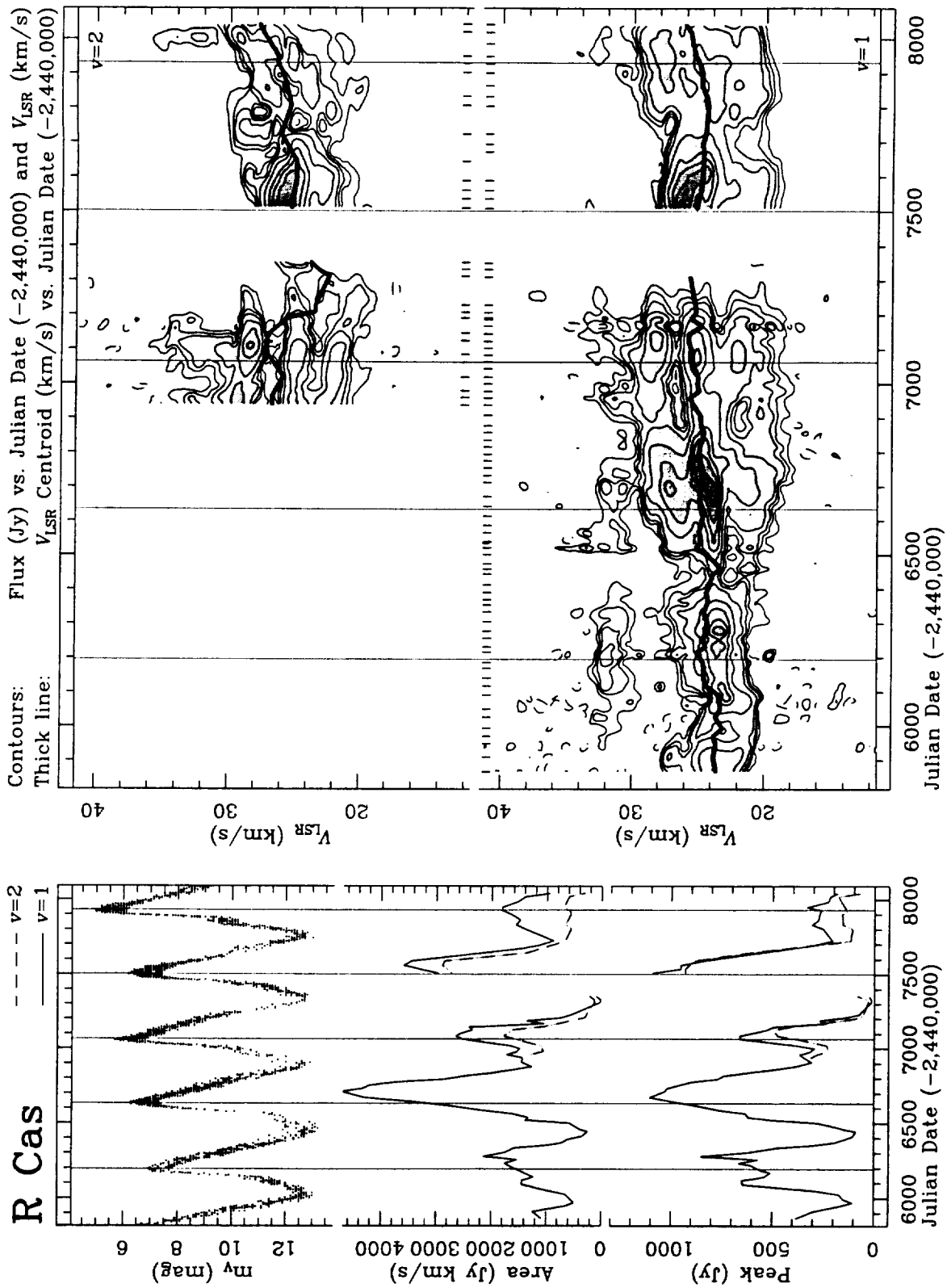

Fig. 11. Same as Fig. 2 for the Mira variable R Cas. v=1 and v=2 contours: −20, 20, 40, 60, 100, 200, 400, 600, 800, and 1000 Jy

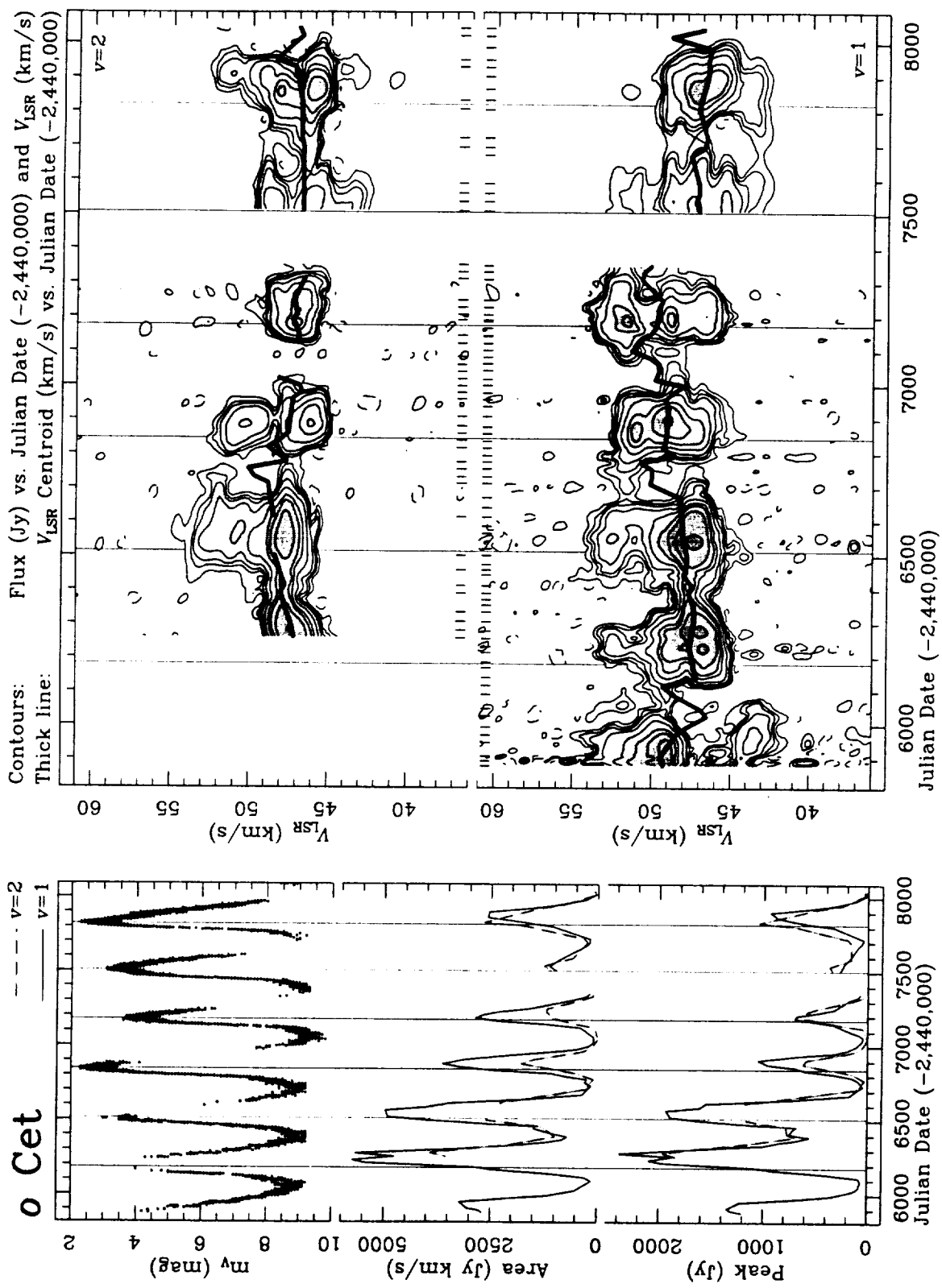

Fig. 12. Same as Fig. 2 for the Mira variable *o* Cet (Mira). v=1 and v=2 contours: −20, 20, 40, 60, 100, 200, 400, 600, 1000, and 2000 Jy

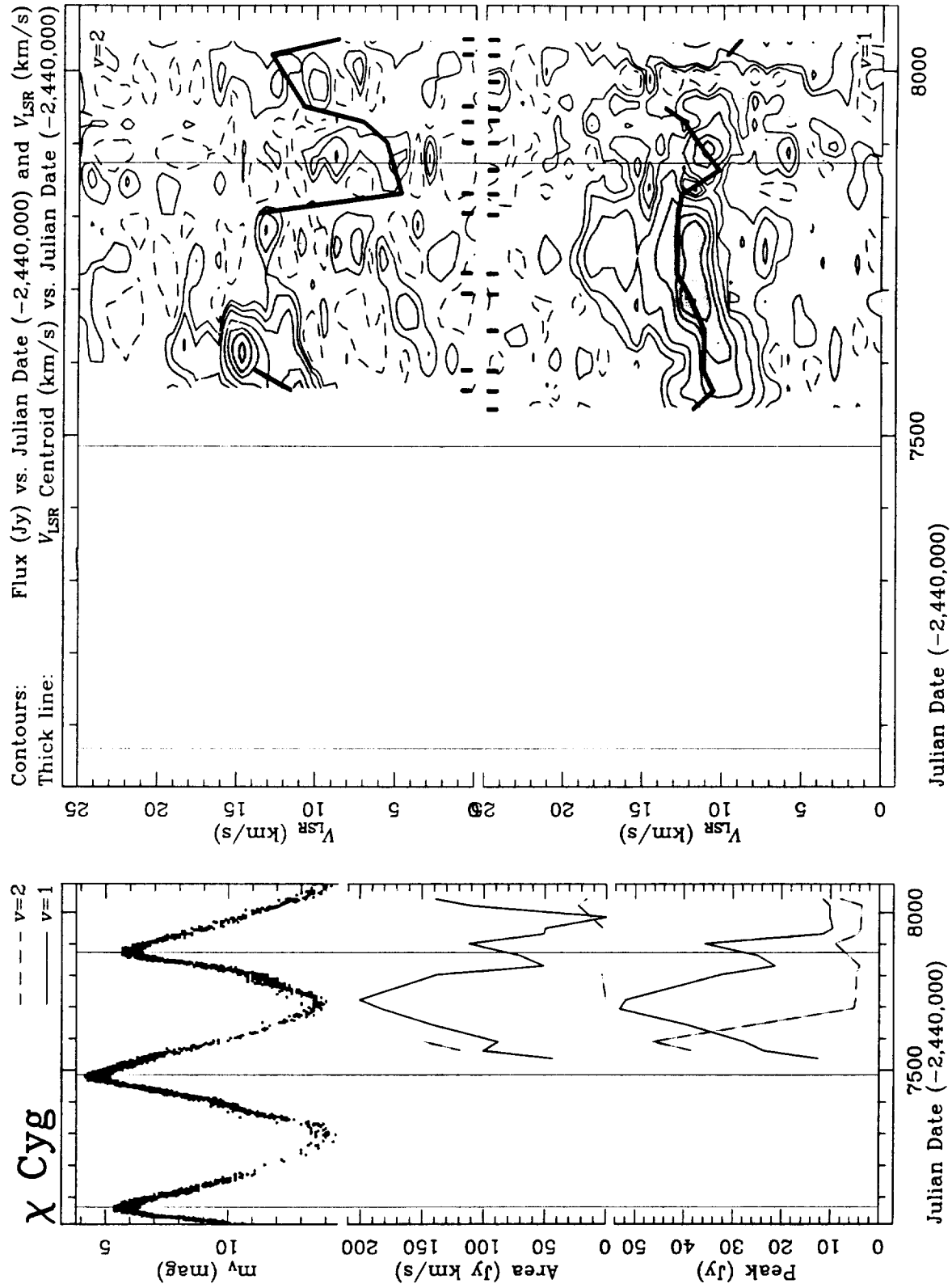

Fig. 13. Same as Fig. 2 for the S-type Mira variable χ Cyg. v=1 and v=2 contours: −2, 2, 5, 10, 20, 30, 40, and 55 Jy

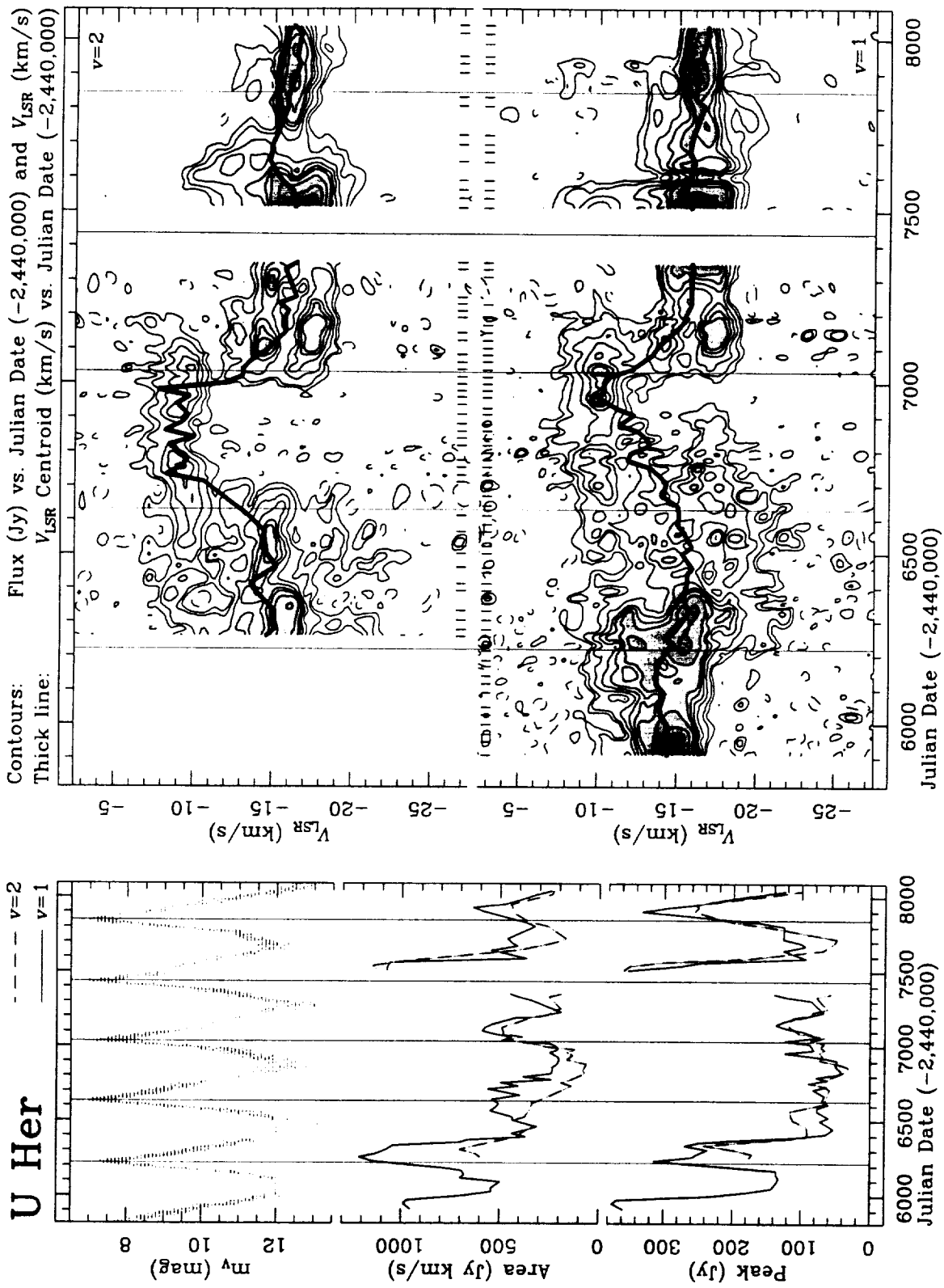

Fig. 14. Same as Fig. 2 for the Mira variable U Her. v=1 and v=2 contours: −10, 10, 20, 40, 60, 80, 100, 150, 250, and 350 Jy

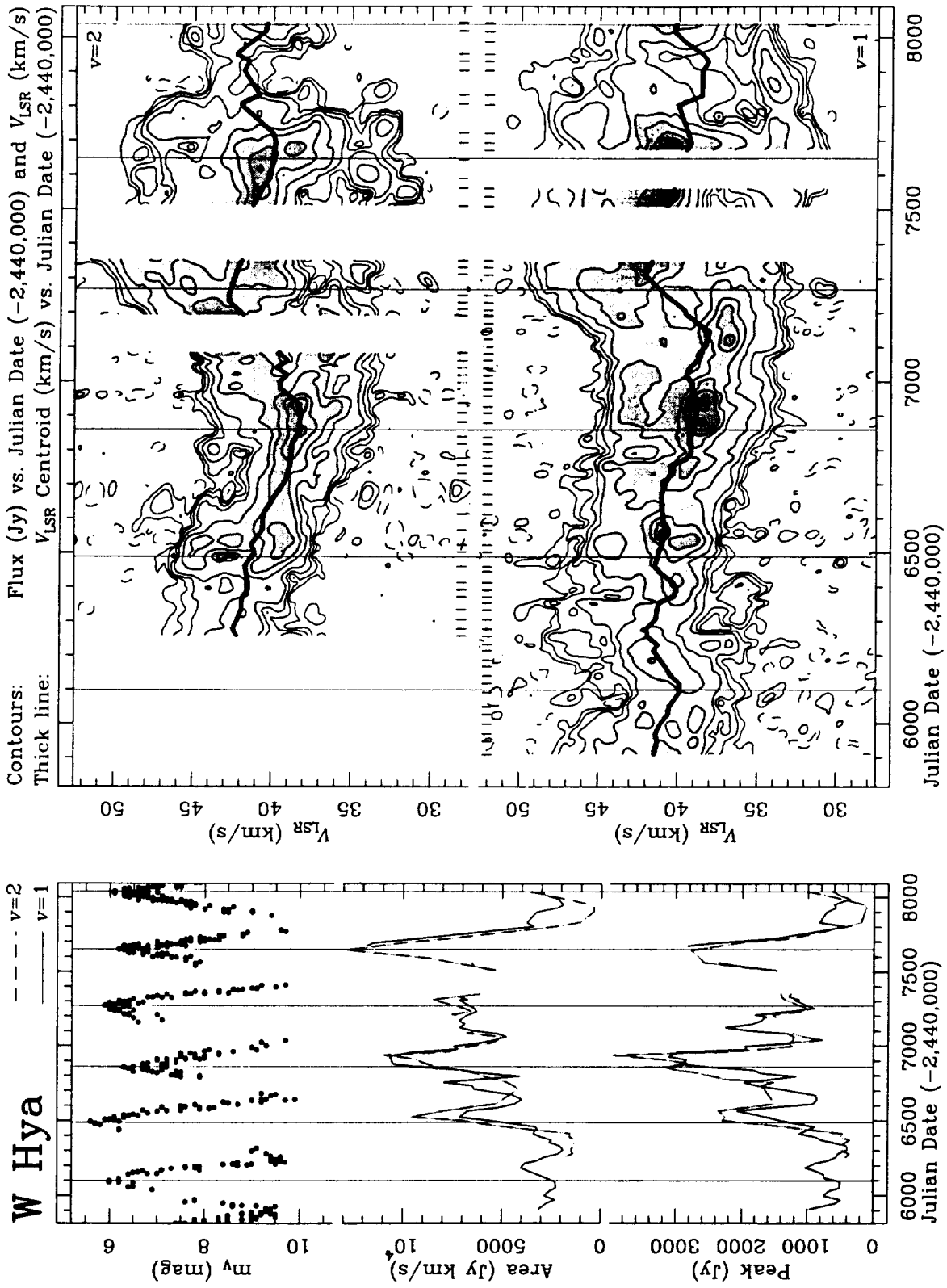

Fig. 15. Same as Fig. 2 for the Mira variable W Hya. v=1 contours: −20, 25, 50, 100, 200, 500, 1000, 1500, 2000, and 3000 Jy. v=2 contours: −20, 25, 50, 100, 200, 500, 1000, 2000, 3000, and 4000 Jy

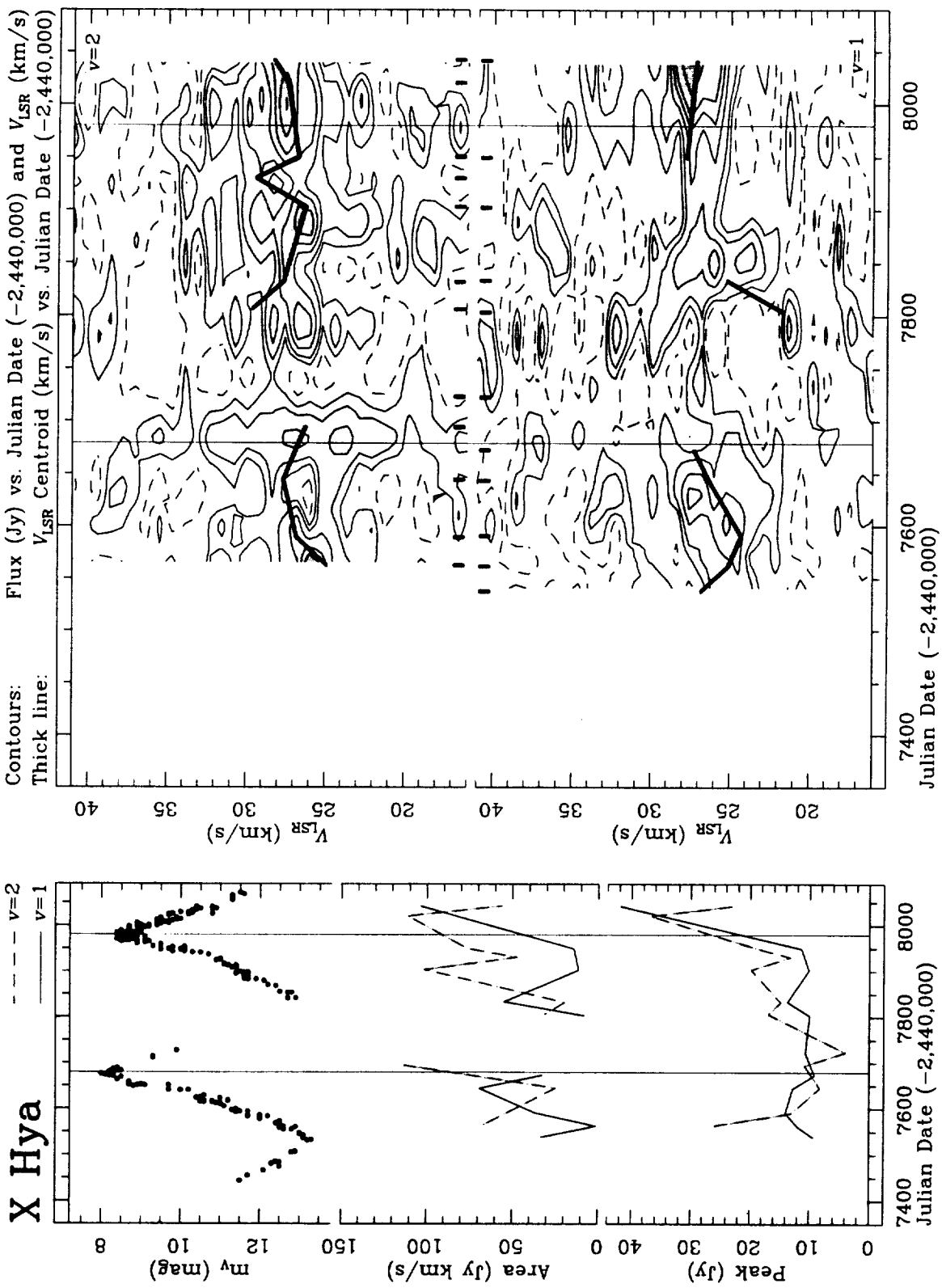

Fig. 16. Same as Fig. 2 for the Mira variable X Hya. v=1 and v=2 contours: −2, 2, 5, 10, 15, 20, 30, and 45 Jy

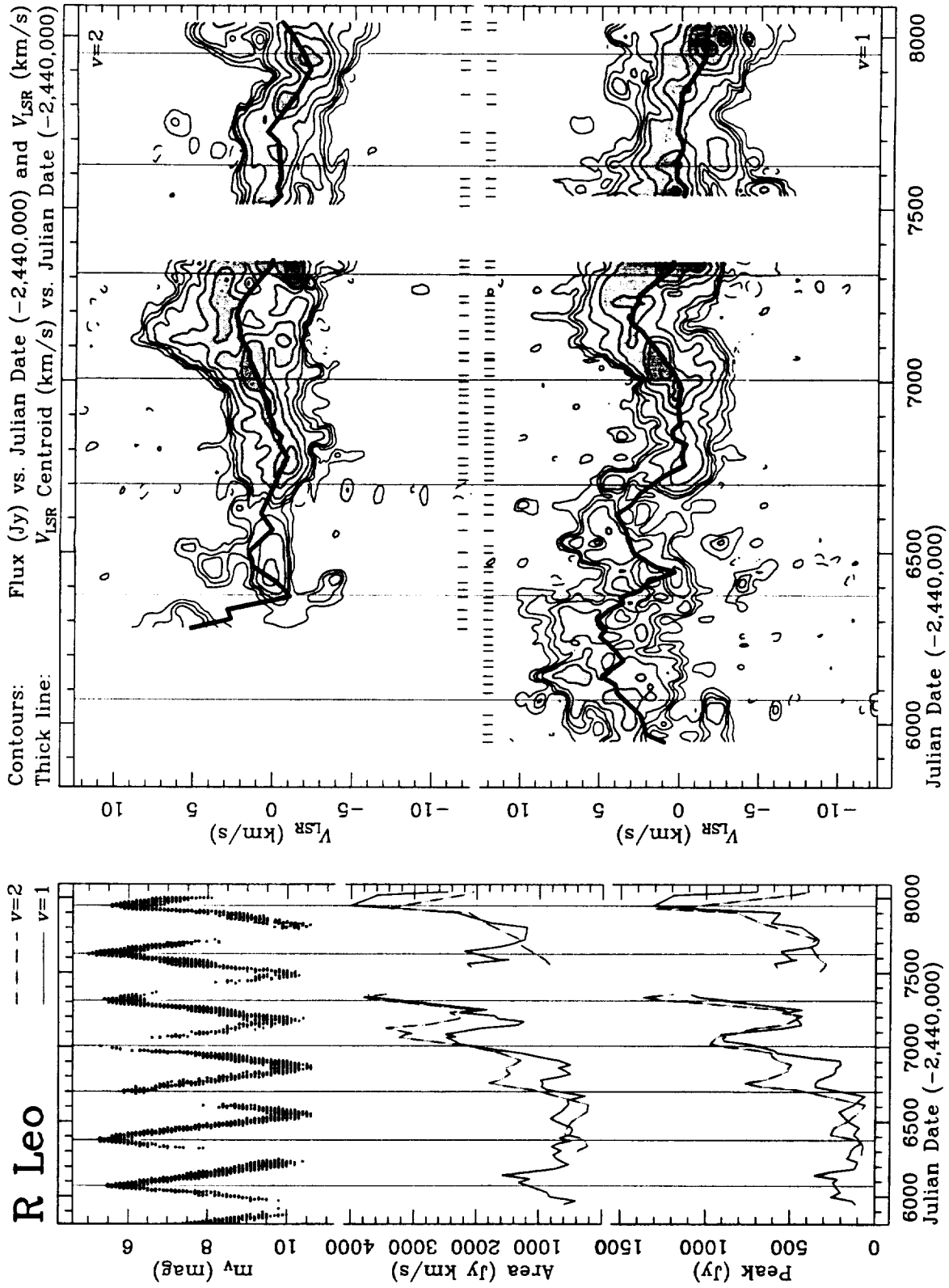

Fig. 17. Same as Fig. 2 for the Mira variable R Leo. v=1 and v=2 contours: −20, 20, 40, 60, 100, 200, 400, 600, 1000, and 1400 Jy

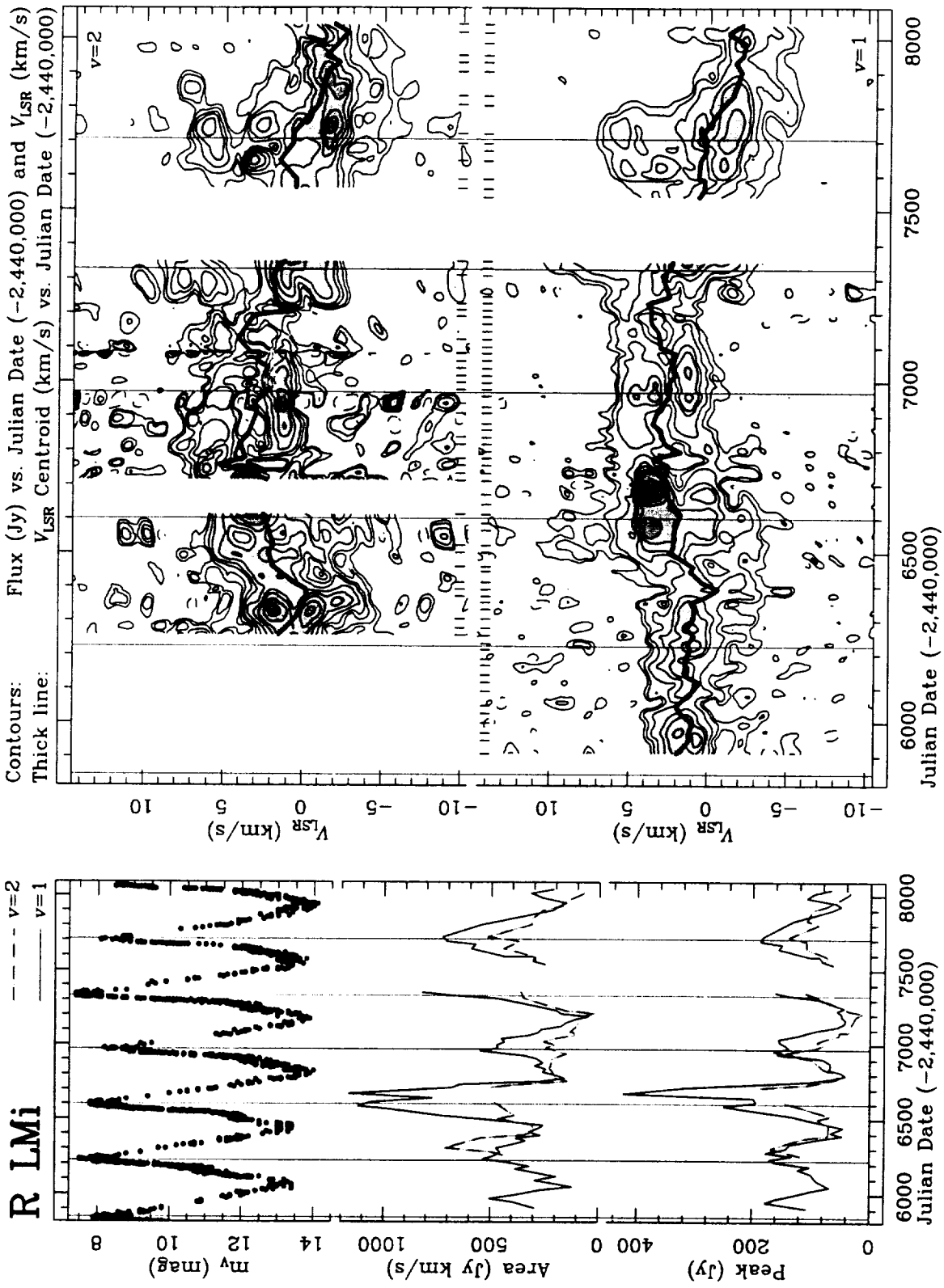

Fig. 18. Same as Fig. 2 for the Mira variable R LMi. v=1 contours: −15, 10, 20, 40, 75, 100, 150, 200, 300, and 400 Jy. v=2 contours: −15, 5, 10, 20, 30, 50, 75, 100, 140, and 180 Jy

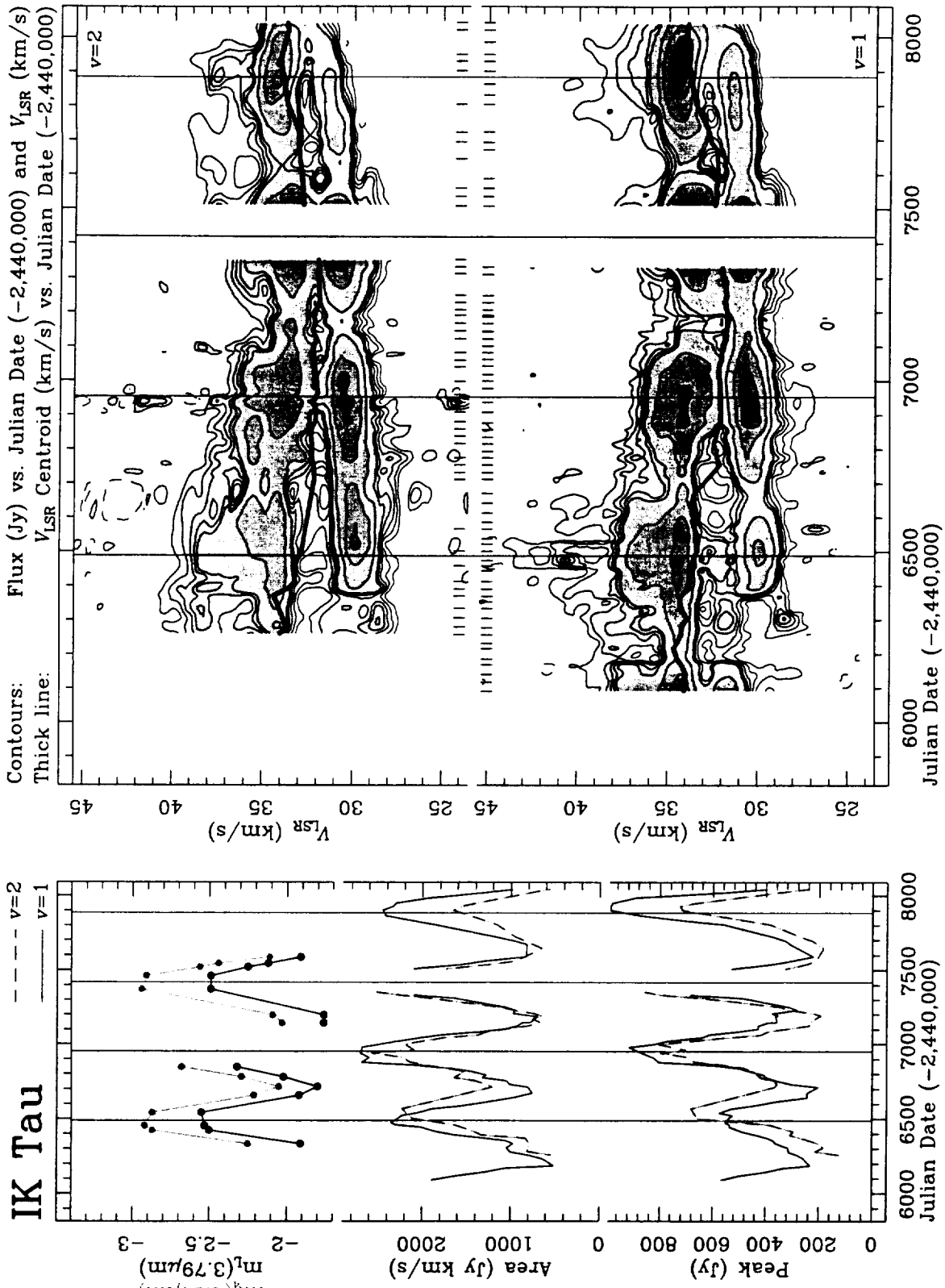

Fig. 19. Same as Fig. 2 for the Mira variable IK Tau (NML Tau). v=1 and v=2 contours: −20, 20, 40, 60, 80, 100, 200, 400, 700, and 900 Jy. The optical magnitude of this star is very weak resulting on poor visible light curves. Thus, the plot includes NIR light curves instead of optical data

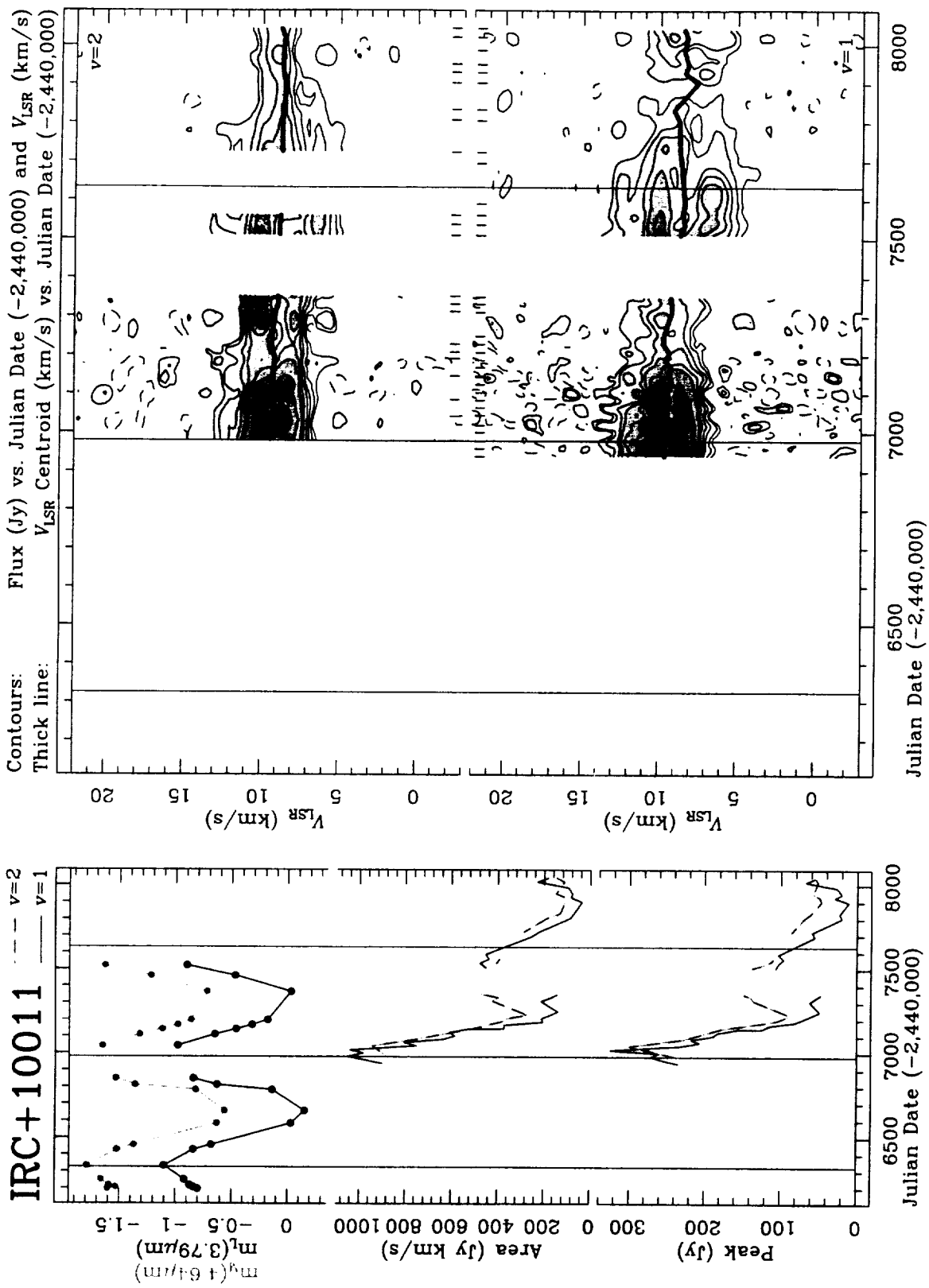

Fig. 20. Same as Fig. 2 for the infrared source IRC +10011 (WX Psc). v=1 and v=2 contours: −10, 10, 20, 40, 60, 90, 120, 180, 250, and 350 Jy. No optical data are available for this star in the AAVSO international data base. NIR light curves corresponding to our observing period are plotted instead

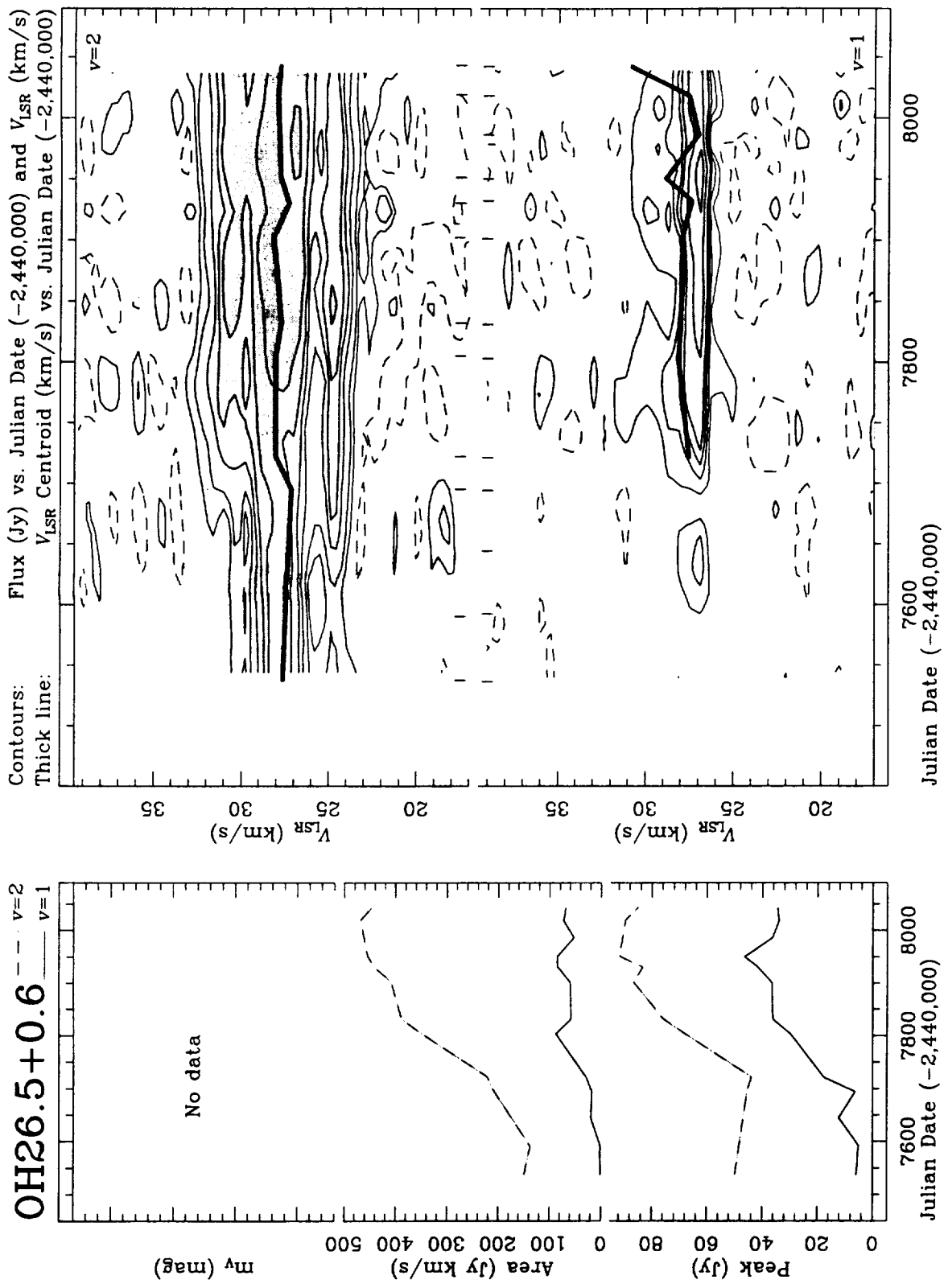

Fig. 21. Same as Fig. 2 for the OH/IR star OH 26.5+0.6. v=1 contours: −3, 5, 10, 15, 20, 30, 40, and 55 Jy. v=2 contours: −3, 5, 10, 20, 30, 40, 60, and 90 Jy. No optical neither NIR variability curves are available for this object

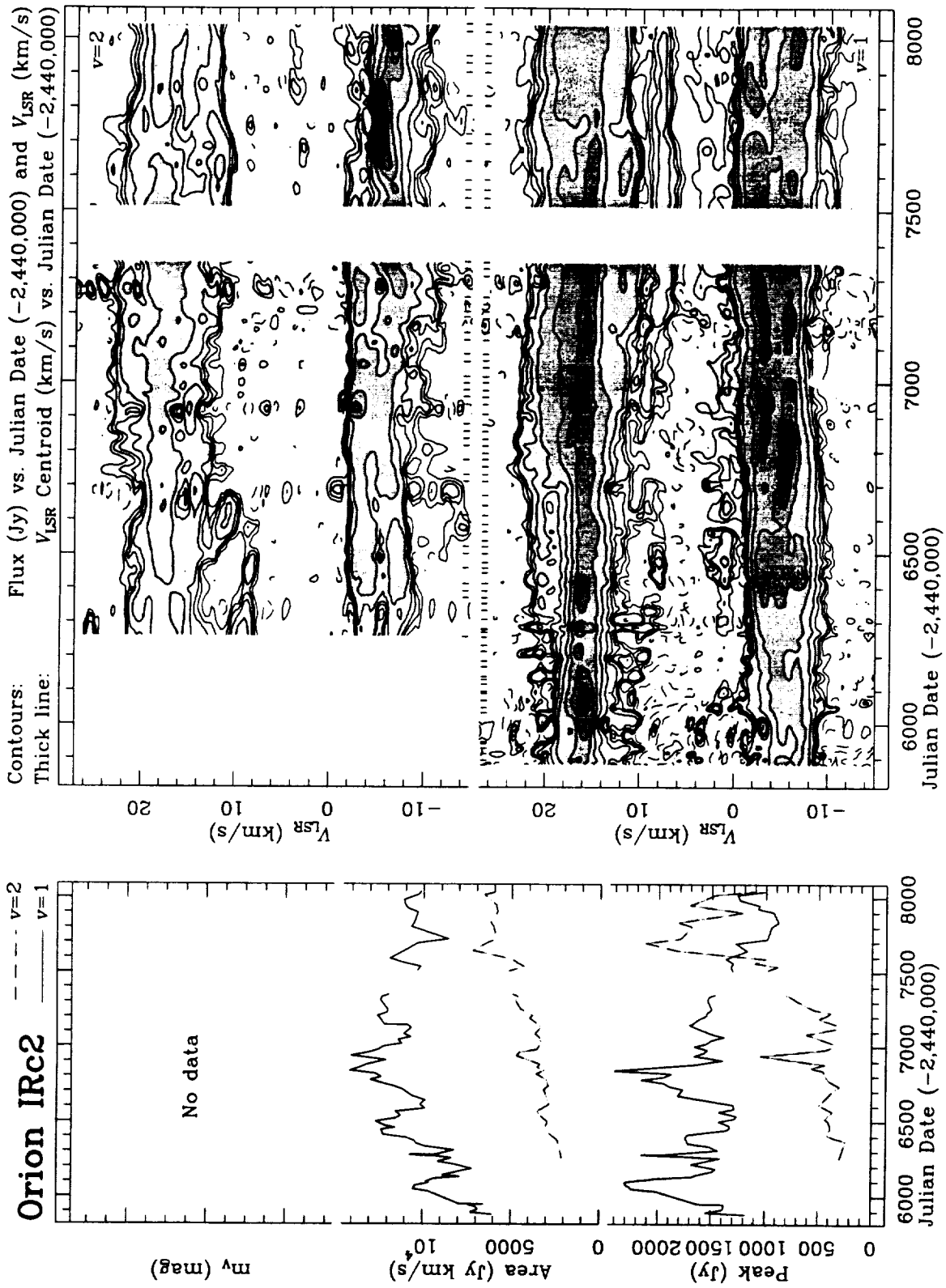

Fig. 22. Same as Fig. 2 for the young stellar source Orion IRc2. v=1 and v=2 contours: −20, 20, 40, 60, 100, 200, 500, 1000, 1500, and 2000 Jy. No velocity centroid curve is shown in this case